



---

**Preparation of Solvent-Dispersible Graphene and its Application to Nanocomposites**

**Soo-Young Park  
Kyungpook National University**

---

**06/14/2016  
Final Report**

**DISTRIBUTION A: Distribution approved for public release.**

**Air Force Research Laboratory  
AF Office Of Scientific Research (AFOSR)/ IOA  
Arlington, Virginia 22203  
Air Force Materiel Command**

REPORT DOCUMENTATION PAGE				Form Approved OMB No. 0704-0188	
<p>The public reporting burden for this collection of information is estimated to average 1 hour per response, including the time for reviewing instructions, searching existing data sources, gathering and maintaining the data needed, and completing and reviewing the collection of information. Send comments regarding this burden estimate or any other aspect of this collection of information, including suggestions for reducing the burden, to Department of Defense, Executive Services, Directorate (0704-0188). Respondents should be aware that notwithstanding any other provision of law, no person shall be subject to any penalty for failing to comply with a collection of information if it does not display a currently valid OMB control number.</p> <p>PLEASE DO NOT RETURN YOUR FORM TO THE ABOVE ORGANIZATION.</p>					
1. REPORT DATE (DD-MM-YYYY) 14-06-2016		2. REPORT TYPE Final		3. DATES COVERED (From - To) 14 May 2014 to 13 May 2016	
4. TITLE AND SUBTITLE Preparation of Solvent-Dispersible Graphene and its Application to Nanocomposites				5a. CONTRACT NUMBER	
				5b. GRANT NUMBER FA2386-14-1-4041	
				5c. PROGRAM ELEMENT NUMBER 61102F	
6. AUTHOR(S) Soo-Young Park				5d. PROJECT NUMBER	
				5e. TASK NUMBER	
				5f. WORK UNIT NUMBER	
7. PERFORMING ORGANIZATION NAME(S) AND ADDRESS(ES) Kyungpook National University 1370 SANGYUCK-DONG BUK-GU TAEGU, 702701 KR				8. PERFORMING ORGANIZATION REPORT NUMBER	
9. SPONSORING/MONITORING AGENCY NAME(S) AND ADDRESS(ES) AOARD UNIT 45002 APO AP 96338-5002				10. SPONSOR/MONITOR'S ACRONYM(S) AFRL/AFOSR IOA	
				11. SPONSOR/MONITOR'S REPORT NUMBER(S) AFRL-AFOSR-JP-TR-2016-0070	
12. DISTRIBUTION/AVAILABILITY STATEMENT Distribution Code A: Approved for public release, distribution is unlimited.					
13. SUPPLEMENTARY NOTES					
14. ABSTRACT Solid-state powders of water-dispersible graphene (GPN) were prepared by treatment of methylmorpholine N-oxide monohydrate (NMMOm). Re-dispersion of GPN in water by simple sonication was successfully demonstrated with a highly concentrated aqueous GPN solution after centrifugation. The produced GPN had the graphitic structure without defects, and its electrical conductivity was 94.7 S/cm, as measured from a filtered GPN film. The spin-coated thin film from the aqueous GPN solution exhibited a single-layered structure. The GPN was also dispersible in polar solvents such as dimethyl sulfoxide, dimethylformamide, ethanol, and tetrahydrofuran. The origin of good dispersity of GPN in polar solvents, including water, was discussed with reference to the high polar nature of NMMO. A nanocomposite system with a water-soluble poly(3,4-ethylenedioxythiophene): poly(styrenesulfonate) (PEDOT:PSS) was prepared on a glass substrate. A four-fold improvement in the electrical conductivity of PEDOT:PSS without deterioration of the transmittance was achieved by adding 1 wt% GPN. The aqueous GPN solution was also utilized as the reaction medium for the in situ polymerization of pyrrole to produce the polypyrrole (PPy)/graphene nanocomposite. The capacitance of PPy measured from cyclic voltammetry (CV) was improved from 122.8 to 278.6 F/g by loading 1 wt% GPN onto the nanocomposite. The capacitance of PPy after 1000 CV cycles was improved from 54.0% to 91.0% by loading 3 wt% GPN onto the nanocomposite. This improvement in the capacitance and capacitance-stability is due to the in situ formation of PPy in the well-dispersed aqueous graphene solution. Thus, this simple preparation of PPy/GPN and PEDOT:PSS/GPN demonstrated the potential for the diverse applications of water-dispersible GPN in various water-based systems such as conducting inks, silver wires, and water-soluble conducting poly					
15. SUBJECT TERMS Graphene, Nanocomposites, Processing					
16. SECURITY CLASSIFICATION OF:			17. LIMITATION OF ABSTRACT	18. NUMBER OF PAGES 27	19a. NAME OF RESPONSIBLE PERSON CASTER, KENNETH
a. REPORT Unclassified	b. ABSTRACT Unclassified	c. THIS PAGE Unclassified			19b. TELEPHONE NUMBER (Include area code) +81-42-511-2000

# Final Report for AOARD Grant FA2386-14-1-4041 “Preparation of Solvent-Dispersible Graphene and its Application to Nanocomposites”

2015-06-13

**PI and Co-PI information:** Soo-Young Park; psy@knu.ac.kr; Kyungpook National University; Department of Polymer Science and Engineering; 80 Daehak Ro, Buk-gu, Daegu 41566, South Korea; Phone: +82-53-950-5630; Fax: +82-53-950-6623.

**Period of Performance:** 05/14/2014 – 05/13/2016

**Abstract:** Solid-state powders of water-dispersible graphene (GPN) were prepared by treatment of methylmorpholine N-oxide monohydrate (NMMOm). Re-dispersion of GPN in water by simple sonication was successfully demonstrated with a highly concentrated aqueous GPN solution after centrifugation. The produced GPN had the graphitic structure without defects, and its electrical conductivity was 94.7 S/cm, as measured from a filtered GPN film. The spin-coated thin film from the aqueous GPN solution exhibited a single-layered structure. The GPN was also dispersible in polar solvents such as dimethyl sulfoxide, dimethylformamide, ethanol, and tetrahydrofuran. The origin of good dispersity of GPN in polar solvents, including water, was discussed with reference to the high polar nature of NMMO. A nanocomposite system with a water-soluble poly(3,4-ethylenedioxythiophene): poly(styrenesulfonate) (PEDOT:PSS) was prepared on a glass substrate. A four-fold improvement in the electrical conductivity of PEDOT:PSS without deterioration of the transmittance was achieved by adding 1 wt% GPN. The aqueous GPN solution was also utilized as the reaction medium for the *in situ* polymerization of pyrrole to produce the polypyrrole (PPy)/graphene nanocomposite. The capacitance of PPy measured from cyclic voltammetry (CV) was improved from 122.8 to 278.6 F/g by loading 1 wt% GPN onto the nanocomposite. The capacitance of PPy after 1000 CV cycles was improved from 54.0% to 91.0% by loading 3 wt% GPN onto the nanocomposite. This improvement in the capacitance and capacitance-stability is due to the *in situ* formation of PPy in the well-dispersed aqueous graphene solution. Thus, this simple preparation of PPy/GPN and PEDOT:PSS/GPN demonstrated the potential for the diverse applications of water-dispersible GPN in various water-based systems such as conducting inks, silver wires, and water-soluble conducting polymers for improving their electron conductivity and stability.

## 1. Introduction:

Graphene combines unique electronic properties and surprising quantum effects with outstanding thermal and mechanical properties.<sup>[1-4]</sup> Several methods to prepare graphene, such as mechanical cleavage of highly ordered pyrolytic graphite (the “scotch tape” method),<sup>[5]</sup> chemical vapor deposition on metals,<sup>[6]</sup> epitaxial growth on SiC or metal substrates,<sup>[7,8]</sup> exfoliation from expanded graphite,<sup>[9,10]</sup> and reduction from graphene oxide (GO),<sup>[11-13]</sup> have been developed. One of these methods, the reduction of GO requires the oxidation of graphite powders to make the precursor of the reduced GO (rGO).<sup>[12,14]</sup> Although the oxidation processes developed can produce relatively large amounts of water-soluble GO compared with the other methods, the resulting GO also exhibits poor electrical and thermal properties due to the presence of many defects, such as wrinkling, crumpling, and atomic vacancies.<sup>[15-17]</sup> Thus, many promising macroscopic applications of graphene require the development of novel routes for producing graphene by effective and direct graphite exfoliation without the need for the oxidation step.

Coleman et al. developed the liquid-phase exfoliation of graphite to transform graphite

into graphene through the sonication of graphite powder in well-selected liquids and aqueous surfactant solutions.<sup>[18,19]</sup> The selection rationale was based on the results of previous theoretical and experimental studies concerning the dispersion of carbon nanotubes in solvents.<sup>[20]</sup> The mechanism underlying the liquid-phase exfoliation process is driven thermodynamically in terms of the enthalpy of mixing for the dissolution of polymers in special liquids as well as the charge-transfer type specific donor-acceptor interactions between the carbon layers of graphite and the solvent molecules.<sup>[18,21]</sup> From the thermodynamic perspective for mixing, organic solvents with surface tensions (or energies) similar to that of graphene (40 to 50 mJ/m<sup>2</sup>) are likely to be an effective dissolution media.<sup>[18,21]</sup> Benzyl benzoate, 1-methyl-2-pyrrolidinone (NMP),  $\gamma$ -butyrolactone (GBL), N,N-dimethylacetamide (DMAc), N-vinyl-2-pyrrolidone (NVP), and N,N-dimethylformamide (DMF), which have surface energies matching that of graphene, could be classified as good exfoliating reagents, whereas others, such as ethanol, acetone, and water, which have surface energies that are significantly lower than that of graphene, are poor media for graphite exfoliation.<sup>[18,19,22]</sup> From the donor-acceptor interaction perspective, a few aromatic and non-aromatic solvents with either strong electron-withdrawing or electron-donating functional groups could be used as media for exfoliating and stabilizing graphene via the charge transfer between the solvent molecules and graphite layers.<sup>[9,22-25]</sup> Such specific interactions would result in carbon atoms with localized charges in graphite not being able to participate in the  $\pi$ -bonding network,<sup>[26]</sup> and significantly weaken the van der Waals attraction between the graphite inter-layers. The efficient exfoliation of graphite in highly ionic media such as ionic liquids<sup>[27,28]</sup> and chlorosulfonic acid (through protonation),<sup>4</sup> are likely driven by the charge transfer mechanism as well.

The solvents mentioned as effective dissolution media tend to be nonvolatile<sup>[29]</sup> because solvents with surface tensions of  $\sim 40$  mJ/m<sup>2</sup> (the Hildebrand solubility parameter approaches 23 MPa<sup>1/2</sup>)<sup>[18,20,26]</sup> have a high boiling point, which can make them difficult to be removed when processing graphene into films or composites.<sup>[18]</sup> In particular, it is virtually impossible to deposit individual flakes from solvent-exfoliated graphene, as aggregation tends to occur during the slow solvent evaporation.<sup>[18]</sup> Although graphene dispersions in high-boiling-point solvents have been transferred into low-boiling point-solvents via solvent exchange,<sup>[22]</sup> it would be preferable to develop a method that allows the direct exfoliation of graphite to provide stable dispersions of graphene in low-boiling-point solvents. This method would greatly simplify graphene exfoliation and significantly expand the number of applications of liquid-exfoliated graphene. Graphene in low-boiling-point solvents, such as chloroform and isopropanol, was demonstrated to be exfoliated at relatively high concentrations with a thickness of less than 10 layers ( $\leq 5$  layers for isopropanol).<sup>[30]</sup> Homogeneous graphene dispersion was also achieved by the removal of aggregates through sonication of graphite in 1-propanol followed by centrifugation.<sup>[31]</sup> However, the concentration of the dispersion was still lower than that from other high-boiling-point solvents; it was possible to achieve concentrations of up to 0.5 mg/mL, which is just less than half of that achieved with high-boiling-point solvents such as NMP.<sup>[30]</sup>

Among low-boiling-point solvents, water would be the best choice as a medium for graphite exfoliation because it is cheap, easily available, and the most environmentally friendly solvent. However, the direct dispersion of hydrophobic graphite or graphene sheets in water without the assistance of dispersing agents has generally been considered an insurmountable challenge. The use of surfactants or hydrophilic organic molecules as dispersing agents is essential for dispersing the graphitic species in water.<sup>[9,19,32-36]</sup> Water-dispersible graphene can be easily applied in inkjet printing, spray- or spin-coating on various substrates and can be used as conductive binders with water-soluble polymers. The direct dispersion of graphene in water is based on the interactions between the dispersing agent and graphene through van der Waals

forces,  $\pi$ - $\pi$  and/or donor/acceptor interactions, and the electrostatic repulsions between the interacted dispersing agents. The dispersing agents can be small molecules or polymers with water-dispersible functional groups such as sodium dodecylbenzenesulfonate (SDBS),<sup>[19]</sup> sodium cholate (SC),<sup>[34]</sup> pluronic P-123,<sup>[35]</sup> 7,7,8,8-tetracyanoquinodimethane (TCNQ),<sup>[9]</sup> pyrenebutyric acid,<sup>[37]</sup> other pyrene (Py) derivatives including 1-pyrene-methylamine (Py-NH<sub>2</sub>) and 1,3,6,8-pyrenetetrasulfonic acid (Py-SO<sub>3</sub>),<sup>[38]</sup> tryptophan,<sup>[39]</sup> rose bengal (RB),<sup>[40]</sup> polyvinylpyrrolidone,<sup>[41]</sup> poly-L-lysine,<sup>[42]</sup> 6-amino-4-hydroxy-2-naphthalenesulfonic acid, and sulfonated polyaniline.<sup>[43]</sup> Recently, Li and co-workers reported that chemically converted graphene sheets could readily form stable aqueous colloids through electronic stabilization in the presence of ammonia.<sup>[44]</sup> However, the use of these dispersing agents for preparing graphene can be a demerit because they can act as impurities in further applications. Thus, methods for preparing water-dispersible graphene without dispersing agents are highly desirable. Lu and coworkers developed a simple and rapid method for the high-yield synthesis of graphene flakes of a few layers by treating graphite with chlorosulfonic acid (CSA) and H<sub>2</sub>O<sub>2</sub>.<sup>[7]</sup> The graphite immediately undergoes dramatic volume expansion upon treating with CSA and H<sub>2</sub>O<sub>2</sub> with the release of a significant amount of heat upon mixing CSA and H<sub>2</sub>O<sub>2</sub> because of the formation of Caro's acid.<sup>[8]</sup> The products formed a highly concentrated dispersion (3 mg/mL) in CSA that was stable for one week without any floating or precipitated particles. However, the direct dispersion of hydrophobic graphite or graphene sheets in water without the assistance of dispersing agents has generally been considered an insurmountable challenge.

N-methylmorpholine N-oxide (NMMO) monohydrate (NMMOm) has a water content between 13.3 and ~17 wt% and a melting point of 76 °C. Its liquid form at ~ 80 °C has been used as an organic solvent that is able to dissolve natural polymers in the industry of man-made regenerated cellulose fibers using the so-called "Lyocell" process.<sup>[45-48]</sup> The chemical structure of NMMO (as shown in Figure 1) has a high electron density on the oxygen, which is able to disrupt the hydrogen bonding in cellulose, causing a decrease in its crystallinity. The highly polar N-O bond (dipole moment of 4.38 mD) in NMMO allows NMMO to become extremely soluble in water by forming hydrogen bonds with water.<sup>[49]</sup> The N-O bond in NMMO can be readily broken and releases a relatively large energy of 222 kJ/mol upon cleavage. NMMO is a strong oxidant, thermally labile, and sensitive toward all types of catalysts that induce N-O bond cleavage. NMMO is a weak basic compound (pK<sub>B</sub> = 9.25); the negatively charged exo oxygen acts as the proton acceptor. Importantly for this research, the surface tension of NMMOm is 44 mJ/m<sup>2</sup> at 80 °C,<sup>[50]</sup> which is well matched with that of the nanotube/graphite (40–50 mJ/m<sup>2</sup>).<sup>[51-54]</sup> Thus, these close values between them lead to a complete miscible state such that the energy cost for exfoliation should be small compared with that for other solvents. Moreover, NMMO is non-toxic, inexpensive, and recyclable for industrial applications.

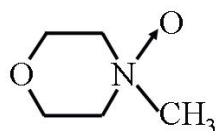


**Figure 1.** Chemical structure of NMMO.

In this work, NMMOm was employed as an exfoliating agent of graphite with CSA/H<sub>2</sub>O<sub>2</sub> treatment. Its close surface tension to graphite, the highly polar nature of the N-O bond, and the proton-acceptor property make it an ideal candidate. More importantly, the obtained graphene (GPN) could be dispersible in water at a high concentration, which opens the path toward new applications in inkjet printing, spray or spin-coating on various substrates for an optovoltaic cell, organic light-emitting diodes, and touch screen panels. To demonstrate the application of the

prepared water-soluble graphene in a nanocomposite system, the water-soluble poly(3,4-ethylenedioxythiophene): poly(styrenesulfonate) (PEDOT:PSS) was hybridized with GPN in water by simple sonication, followed by spin-coating on a glass substrate. The PEDOT:PSS/GPN thin film exhibited good dispersity of GPN in the PEDOT:PSS polymer matrix and improved electrical conductivity. The GPN was also used in the in situ polymerization of PPy. The PPy/GPN nanocomposite system showed improved capacitance with good capacitance stability, too.

## **2. Experiment:**

**2-1. Materials:** Graphite powder (< 20  $\mu\text{m}$ , synthetic), sulfuric acid ( $\text{H}_2\text{SO}_4$ ), hydrochloric acid ( $\text{HCl}$ ), hydrogen peroxide ( $\text{H}_2\text{O}_2$ ), potassium permanganate ( $\text{KMnO}_4$ ), and sodium nitrate ( $\text{NaNO}_3$ ) were purchased from Sigma-Aldrich Inc. NMMOm (which was evaporated from a 50 wt% aqueous solution of BASF© NMMO) was supplied by Kolon©. PEDOT:PSS (PH1000) (the solid content is 1 wt% in water) was purchased from Clevios™. Isopropyl alcohol (IPA) and sodium hydroxide ( $\text{NaOH}$ ) were purchased from Junsei Chemical. Dimethyl sulfoxide (DMSO), dimethylformamide (DMF), ethanol, tetrahydrofuran (THF), dichloromethane (DCM), toluene, trichloroethylene (TCE), and n-hexane were obtained from Duksan Pure Chemicals Co., Ltd. (South Korea), chlorosulfonic acid (CSA, Wako Pure Chemical Industries Ltd., Japan), sodium hydroxide ( $\text{NaOH}$ , Duksan Pure Chemicals Co., South Korea), pyrrole ( $\text{C}_4\text{H}_5\text{N}$ , Daejung Chemicals & Metals Co., Ltd, South Korea), iron (III) chloride ( $\text{FeCl}_3$ , Junsei Chemical, Japan), hydrazine ( $\text{N}_2\text{H}_4$ , Junsei Chemical, Japan), expanded graphite (EG) powder (EG, <100  $\mu\text{m}$ , C-Therm 001, Timcal C&G Inc, Switzerland), graphite powder (<100  $\mu\text{m}$ , Timrex BNB 90, Timcal C&G Inc., Switzerland), and potassium chloride ( $\text{KCl}$ , Junsei Chemical, Japan) were used as-received.

**2-2. CSA and  $\text{H}_2\text{O}_2$  treatment:** EG (5 g) was added to a 500 mL one-necked round-bottomed flask containing 200 mL concentrated CSA. After stirring the mixture for 1 day at 25  $^\circ\text{C}$ , 75 mL  $\text{H}_2\text{O}_2$  was slowly added dropwise. The solution reacted vigorously with significant expansion. After the reaction, the mixture was diluted using 3 L distilled water. The diluted mixture was filtered (ADVANTEC, qualitative filter paper No. 2) and washed with large amounts of water until the solution was at pH 7, to remove CSA completely. The filtered graphite powders (CSA-treated graphite) were dried in an oven at 60  $^\circ\text{C}$ .

**2-3. Preparation of GPN:** NMMOm (550 g) was melted at 90  $^\circ\text{C}$  in a cylindrical tube (diameter of 6 cm and length of 20 cm). After melting, the graphite powders (or CSA-treated graphite) (3 g, 0.54 wt%) were placed into the tube, and then, the tip of a horn-type sonicator (VCX-750, Sonics & Materials, Inc. Vibracell™, USA, 750 W and 20 Hz) was inserted into the tube. For 2 h, the NMMO/graphite dope was sonicated at 90  $^\circ\text{C}$ . After sonication, the NMMO/graphite (or CSA-treated graphite) dope was diluted with water (3 L). The diluted solution was left for 24 h to allow the supernatant and sediment parts to separate. The supernatant part was carefully decanted. The decanted part was centrifuged at 3,000 rpm for 30 min using a centrifuge (Vision Scientific Co., VS-21SMTN, Korea). Its supernatant part after centrifugation was subjected to a second centrifugation under the same conditions. After centrifugation and decanting,  $\text{NaOH}$  (2 g) was added to the supernatant part to precipitate the graphene. After 1 d, the precipitated graphene was filtered with large amounts of water (~ 3 L) on a cellulose filter (ADVANTEC®, cellulose membrane filter, 0.2- $\mu\text{m}$  pore size) until the solution reached pH 7. NMMO and  $\text{NaOH}$  were completely removed during filtration, and the black powders (GPN (for graphite powder), eGPNc ((or CSA-treated graphite))) could be gathered on the filter, which were dried in a vacuum

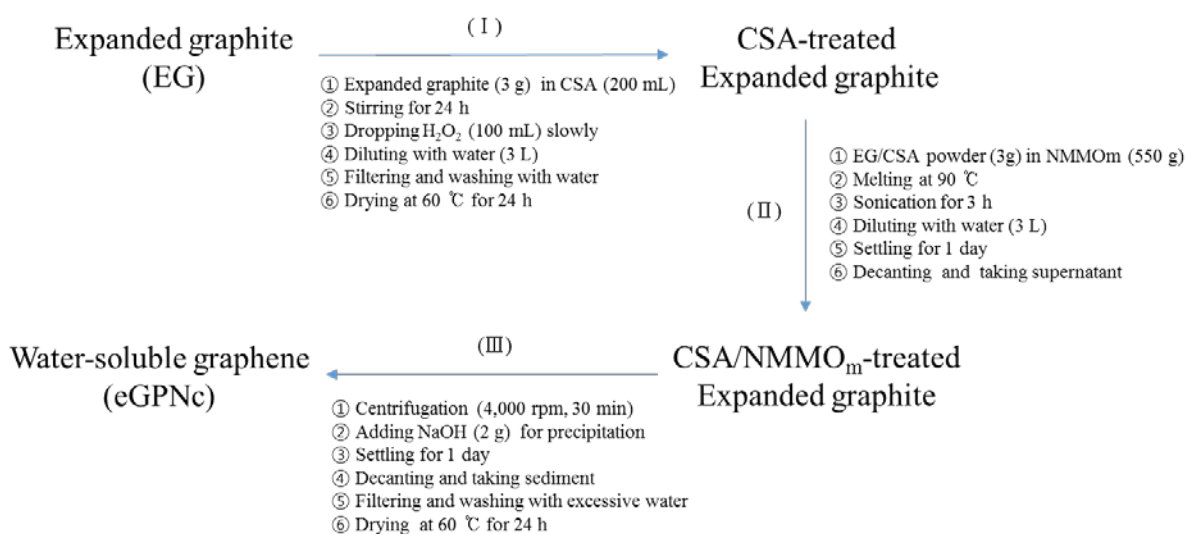
oven at 60 °C.

**2-4. Preparation of graphene film:** The graphene film was prepared by a filtering method. The decanted solution before NaOH addition was filtered on a cellulose filter (ADVANTEC®, cellulose membrane filter, 0.2- $\mu$ m pore size). The uniform free-standing film with a thickness of  $\sim 80$   $\mu$ m was peeled off to separate from the cellulose filter, and its electrical conductivity was measured using a four-point probe.

**2-5. Dispersion in water:** The aqueous dispersion of the GPN powders was performed using the tip of a horn-type sonicator (VCX-750, Sonics & Materials, Inc. Vibracell™, USA, 750 W and 20 Hz) with the aqueous solutions having designated GPN concentrations. All the experiments were performed with 2-h sonication unless otherwise noted. After sonication, the supernatant part was decanted, and its concentration was measured using a UV-Vis spectrometer (V-650, Jasco, Japan) from UV absorbance using the Lambert-Beer law with an absorbance coefficient of 38.008 mL/mg/cm (at 600nm), which was determined from a calibration curve.

**2-6. Preparation of PEDOT:PSS/GPN nanocomposite:** To obtain maximum electrical conductivity of the spin-coated PEDOT:PSS film on the glass substrate, the reported method was employed with IPA and ethanol treatments.<sup>[55,56]</sup> The procedure for the preparation of PEDOT:PSS/GPN nanocomposite thin films on the glass substrate with IPA mixing and ethanol soaking is described in the following text. The aqueous PEDOT:PSS solution (20 g, 1 wt%) was mixed with IPA (5 g) to obtain a 0.8 wt% PEDOT:PSS solution. Then, the predetermined amounts of GPN were added into the PEDOT:PSS/IPA solutions. The PEDOT:PSS/IPA/GPN mixtures were vigorously stirred for 1 d with a magnetic bar and were then sonicated for 2 h using a horn-type sonicator. The sonicated PEDOT:PSS/IPA/GPN solutions were further stirred at 400 rpm for 1 d with a magnetic bar. Then, 0.3 mL of the final PEDOT:PSS/IPA/GPN solutions was spin-coated on the glass substrate in 3 steps (step 1 at 500 rpm for 5 sec, step 2 at 2,000 rpm for 20 sec, and step 3 at 800 rpm for 5 sec).<sup>[57]</sup> The spin-coated PEDOT:PSS/IPA/GPN films were dried at 80 °C on a hot plate for 1 min, and then, 0.5 mL of ethanol was dropped onto the spin-coated PEDOT:PSS/IPA/GPN thin film. The ethanol-soaked PEDOT:PSS/IPA/GPN film was left for 5 min with a glass dish cover and dried at 80 °C on a hot plate.<sup>[58]</sup> The prepared thin films were  $\sim 40$  nm thick.

**2-7. Preparation of GO:** GO was synthesized by oxidizing graphite using the Hummer's method.<sup>14</sup> Briefly, 4 g of raw graphite, 2 g of NaNO<sub>3</sub> and 12 g of KMnO<sub>4</sub> were added to a 500-mL round-bottom flask containing 100 mL of concentrated H<sub>2</sub>SO<sub>4</sub>. The mixture was first cooled by immersion in an ice bath for 1 h with constant stirring and then slowly heated to 35 °C for 3 h. The reaction was quenched by adding 200 mL of deionized (DI) water, and the mixture was left to stand for 30 min. A H<sub>2</sub>O<sub>2</sub> solution (30 %; 3 mL) was then added to reduce the unreacted permanganate. The mixture was then filtered through a cellulose filter and washed sequentially with dilute HCl and DI water. The resulting GO was dried at 60 °C for 48 h.



**Scheme 1.** Schematic procedure for the preparation of water-soluble graphene, eGPNc.

**2-8. PPy/GPN nanocomposite preparation:** PPy/eGPNc nanocomposites were synthesized using in situ synthesis of PPy in the eGPNc aqueous suspension. Pyrrole monomers (0.42 g, 6.25 mM) were added into the 50 mL eGPNc aqueous suspension at concentrations of 0.08–0.44 mg/mL. Then, 6.25 mM  $\text{FeCl}_3$  solution (6.76 g) was slowly added into the above mixture and kept at 0–4 °C for 24 h. Finally, the reaction mixture was filtered and washed with methanol and ethanol, and the final product was dried in an oven at 60 °C for 24 h. For comparison, pure PPy was prepared without graphene using a similar procedure.

## 2-9. Measurements:

**SEM and AFM:** A sonicated dilute aqueous GPN solution (0.001 mg/mL, 2 mL) was spin-coated at 1,000 rpm on the  $\text{O}_2$  plasma-treated silicon wafer and dried completely for scanning electron microscopy (SEM, S-4800, Hitachi, Japan) and atomic force microscopy (Nanoscope IIIa, DI instrument, UK) observations.

**XPS:** The powder samples were used for X-ray photoelectron spectroscopy (XPS, VG Microtech, ESCA2000, UK) using an Al  $K\alpha$  X-ray source (1486.6 eV) in the range of 0 to 800 eV.

**Four-point probe:** The sheet resistance of the spin-coated films and electrical conductivity of the free-standing graphene film at room temperature were measured using a four-point probe in combination with a source meter (2400, Keithley, USA).

**FT-IR:** Fourier-transform infrared spectroscopy (FTIR, FT/IR-620 unit, Jasco, Japan) was performed under vacuum. The FT-IR samples were vacuum-dried for 1 d, mixed with KBr, and pressed into 13-mm-diameter pellets. The spectra with a  $1\text{ cm}^{-1}$  resolution were derived from 50 scans.

**Raman:** Raman spectroscopy at 600 to 4000  $\text{cm}^{-1}$  was performed using a Raman spectrometer (NT-MDT, NTEGRA spectra, Russia) with backscattering geometry and excitation at 532 nm of an argon laser. The specimens for Raman spectroscopy were prepared by filtering the powder samples, peeling the films from the filter paper, and drying.

**UV/Vis:** The transmittance of the aqueous GPN solutions was measured using a UV/Visible spectrophotometer (V-650, Jasco, Japan).

**Zeta Potential:** The zeta potential and size of GPN in water were measured with a dynamic light scattering instrument (ZEN3690, MALVERN, UK) at a 0.001 mg/mL concentration.

**Turbiscan:** The stability of the GPN dispersions in water was determined using Turbiscan (Turbiscan™ Lab Expert, Formulaction©, France) with the GPN aqueous solutions (0.001 mg/mL) sonicated for 2 h by a horn-type sonicator before the measurements. The solution transmittance for Turbiscan was measured along the vial height (range 5 to 35 mm) at  $\lambda = 880$  nm every 30 min for 24 h and then every 1 d. The transmittance along the height at a certain time was averaged to obtain a graph of the transmittance as a function of time.

**TEM and Electron diffraction:** Scanning transmission electron microscopy (STEM, Titan G2 ChemiSTEM Cs Probe, FEI, Netherlands) was performed at 200 kV to obtain the GPN images with selected area electron diffraction (SAED) of the drop-cast samples of the aqueous solutions (0.001 mg/mL) on lacey carbon grids (TED PELLA, Inc., 200 mesh, Cu). The colloidal dispersion was studied with a He-Ne laser beam at 632.8 nm to observe the Tyndall effect.

**X-ray:** The WAXD measurements were conducted at the PLS-II U-SAXS beamline of the Pohang Accelerator Laboratory (PAL) in Korea. The X-rays originating from the in-vacuum undulator (IVU) were monochromatized using Si(111) double crystals and focused at the detector using K-B type mirrors. Wide-angle X-ray diffraction (WAXD) patterns were recorded with a 2D CCD detector (Rayonix SX165), and the X-ray irradiation time was 20 s. Diffraction angles were calibrated using pre-calibrated sucrose (Monoclinic, P21,  $a = 10.86$  Å,  $b = 8.70$  Å,  $c = 7.76$  Å,  $\beta = 102.94^\circ$ ) and the sample-to-detector distance (SDD) was about 233.43 mm.

**Potentiometer:** Galvanostatic charge–discharge (GCD), cyclic voltammetry (CV), and impedance properties were measured using a potentiometer (PARSTAT 4000-PLUS, AMTEK Princeton Applied Research, USA). The sample preparation procedures for these electrical-property measurements are as follows. The PPy (or PPy/eGPNc) sample was completely mixed with carbon black (Super P, Alfa Aesar, Great Britain) and poly(tetrafluoroethylene) (PTFE) binder by grinding using a mortar with the addition of small amounts of ethanol for fluidity. The mixture sample was hot-pressed into 100- $\mu$ m thick films. Samples with a size of  $1 \times 1$  cm<sup>2</sup> were cut and dried in an oven at 60 °C for ~2 h. This film was adhered to indium tin oxide (ITO) glass with silver paste for measuring electrical properties.

### 3. Results and Discussion:

**3-1. Preparation of water-soluble graphene:** In order to study the effect of the CSA/H<sub>2</sub>O<sub>2</sub> treatment on the yield of the water-dispersible graphene, the yield of the eGPNc was compared with that of GPN, which was produced using the same method without the CSA/H<sub>2</sub>O<sub>2</sub> treatment.<sup>[85]</sup> Expanded and normal graphite powders were also tested together to determine the effect of the layer expansion of the raw graphite powders on the yield of graphene. GPN and GPNc were produced from normal graphite powders, and eGPN and eGPNc were produced from EG powders. GPN and eGPN were produced without the CSA/H<sub>2</sub>O<sub>2</sub> treatment, and GPNc and eGPNc were produced with the CSA/H<sub>2</sub>O<sub>2</sub> treatment. Table SI 1 shows the yields of the produced graphenes. The yields of GPN, eGPN, GPNc, and eGPNc are 0.6, 0.8, 0.9, and 3.0 wt%, respectively. The CSA/H<sub>2</sub>O<sub>2</sub> treatment increases yield more than three times when the EG powers were used as a raw material (0.8 wt% (eGPN) vs. 3.0 wt% (eGPNc)), and the EG is effective for high yield (0.9 wt% (GPNc) vs. 3.0 wt% (eGPNc)). The 3.0 wt% yield is quite high compared to other reported yields. For example, yield of graphene obtained from the NMP treatment is ~1 wt%.<sup>2</sup>

**Table 1.** Measured graphene yields using different methods; GPN and GPNc were produced from normal graphite powders, and eGPN and eGPNc were produced from expanded graphite powders; GPN and eGPN were produced without the CSA/H<sub>2</sub>O<sub>2</sub> treatment and GPNs and eGPNs

were produced with the CSA/H<sub>2</sub>O<sub>2</sub> treatment; (II)-⑤ and (III)-① represent powders at the steps (II)-⑤ and (III)-① in Scheme 1, respectively.

	Initial (g)	(II)-⑤ (g)	(III)-① (g)	Final (g)	Yield (%)
GPN	3	2.895	0.048	0.017	0.6
eGPN	3	2.507	0.117	0.024	0.9
GPNc	3	2.818	0.094	0.026	0.9
eGPNc	3	2.626	0.224	0.088	3.0

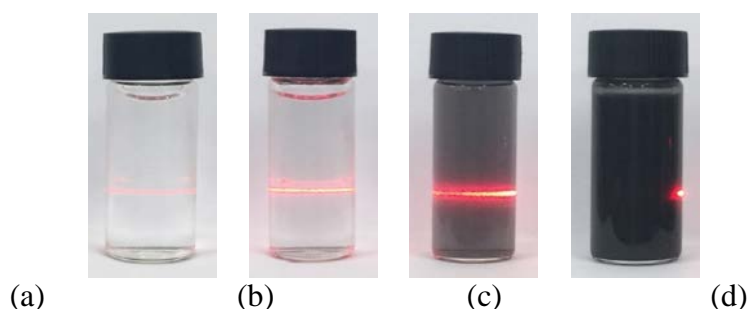


**Figure 1.** Photographs of the dispersion of eGPNc in water after sonication for 2 h with different concentrations ( $C_{\text{eGPNc}}$ ) of (a) 0.001, (b) 0.01, (c) 0.1, and (d) 1 mg/mL; the laser beams (coming from the right) in the vials are used to observe the Tyndall effect.

### 3-2. Dispersity of GPN in water

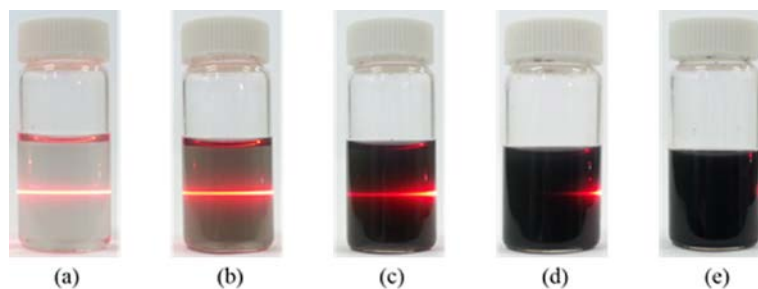


**Figure 2.** Photographic images of the dispersion of GPN in water after sonication for 2 h with different concentrations ( $C_{\text{GPN}}$ ) of (a) 0.001, (b) 0.01, (c) 0.1, (d) 1, and (e) 3 mg/mL; the laser beams in the vials are used to observe the Tyndall effect.

Re-dispersion of the dried GPN powders in water was performed. Re-dispersion of dried powers has many merits because the exact amount of the GPN in a solvent can be controlled by weight (not by the volume of the solution). In addition, the solid-state GPN powders are more convenient to store than GPN in the solution state. Figures 2 a-e show photographs of the dispersion of GPN in water after sonication for 2 h with different concentrations ( $C_{\text{GPN}}$ ) until 3 mg/mL. The black color is observed for the aqueous GPN solution (instead of the brown color of the aqueous GO solution) and becomes darker as  $C_{\text{GPN}}$  increases. No sediment was visible on the bottom of the vial. The clear straight laser beams in the vials due to the Tyndall effect indicate

that the colloidal particles of the GPN were dispersed well in the water.<sup>[4]</sup> At high  $C_{\text{GPN}}$ s greater than 1 mg/mL, the GPN solution becomes so dark that the laser beam cannot be observed. The GPN solution at  $C_{\text{GPN}} = 0.001$  mg/mL (the lowest concentration) shows no visible precipitation 24 h after sonication, whereas that at  $C_{\text{GPN}} = 0.1$  mg/mL (the highest concentration) exhibits slight precipitation with the supernatant remaining black. Figure supplementary information (SI) 2 presents photographs of the GPN dispersion in water at  $C_{\text{GPN}} = 1$  mg/mL immediately and 3 months after sonication for 2 h. The good dispersion still lasts with small amounts of precipitation, indicating that the dispersion of the GPN in water is stable for a long period.

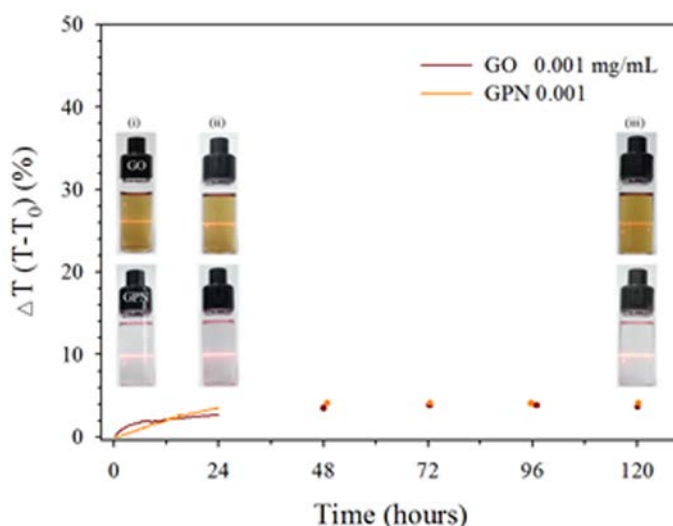


**Figure 3.** Transmission increases ( $\Delta T$ ) of the GPN and GO dispersions measured by Turbiscan as a function of time for 120 h with 0.001 mg/mL of  $C_{\text{GPN}}$  and  $C_{\text{GO}}$  (before 24 h : every 30 min, after 24 h : every 24 h), and (inset) photographs of the GPN and GO (i) immediately and (ii) 24 h and (iii) 120 h after sonication for 2 h; the laser beams in the vials are to see the Tyndall effect.

To quantitate the dispersion of the GPN, Turbiscan was used. The initial transmittances of the GPN and GO dispersions decrease as  $C_{\text{GPN}}$  and  $C_{\text{GO}}$  increase because of the absorption of the beam by the GPN and GO particles. The GPN and GO dispersions at  $\geq 0.1$  mg/mL could not be tested because of the complete blocking (no transmission) of the beam resulting from the high concentration of the solution. The increase of the transmittance ( $\Delta T$ ,  $T - T_0$ ) at a certain period represents the settlement of the particles; thus, a small increase of transmittance indicates stable dispersion of the particles in the solvent during that time. Figure 3 shows  $\Delta T$  for 120 h (before 24 h : every 30 min, after 24 h : every 24 h) for the GPN and GO dispersions.  $\Delta T$  of the GPN (and GO) dispersions increases slightly. However,  $\Delta T$  of the GPN solution is comparable to that of the GO solution, indicating that the GPN exhibits similar dispersity in water as the GO even though there are few chemical functional groups in GPN, which will be discussed later.

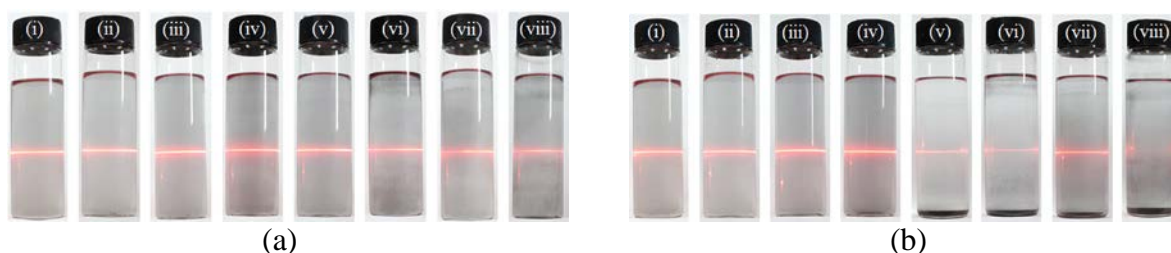


**Figure 4.** Photographs of the GPN dispersion at  $C_{\text{GPN}} = 0.001$  mg/mL in (i) DMSO (7.2), (ii)

DMF (6.4), (iii) ethanol (5.2), (iv) THF (4.0), (v) DCM (3.1), (vi) toluene (2.4), (vii) TCE (1.1), and (viii) *n*-hexane (0.0) (a) immediately and (b) 24 h after sonication for 2 h; the number in parenthesis is the polarity index ; the laser beams in the vials are to see the Tyndall effect.

The GPN dispersion was tested in several organic solvents. The GPN at  $C_{\text{GPN}} = 0.001$  mg/mL was dispersed in different organic solvents by a horn-type sonicator. Figure 4 presents photographs of the GPN dispersion at  $C_{\text{GPN}} = 0.001$  mg/mL in DMSO, DMF, ethanol, THF, DCM, toluene, TCE, and *n*-hexane immediately and 24 h after sonication for 2 h. For the GPN dispersion immediately after sonication for 2 h, the GPN in all the organic solvents was dispersed, which was evidenced by the black color and clear laser beam. However, 24 h after sonication, the GPN in DCM, toluene, TCE, and *n*-hexane shows the settlement of GPN even though the GPN in DMSO, DMF, ethanol, and THF still shows good dispersion. The polarity indices of water, DMSO, DMF, ethanol, THF, DCM, toluene, TCE, and *n*-hexane are 9.0, 7.2, 6.4, 5.2, 4.0, 3.1, 2.4, 1.1, and 0, respectively.<sup>[71]</sup> This result indicates that the polar solvents such as water, DMSO, DMF, ethanol, and THF can disperse the GPN, which might be due to the high polar nature of the GPN powders. The dipole-dipole interactions between GPN and the polar solvent might improve the dispersity of the GPN in the solvents. The origin of the high polarity of GPN is not certain, although the small amounts of NMMO remaining on the GPN after the NMMO treatment might result in a large dispersion effect in the solvent at this moment. The existence of small amounts of NMMO on the GPN will be discussed later. Water is the most polar solvent; thus, the GPN is highly dispersible in water. The aqueous GPN solution at  $C_{\text{GPN}} = 0.001$  mg/mL shows good dispersity with a zeta potential value of - 47.2 mV. According to the American Society for Testing and Materials (ASTM), colloids with zeta potentials higher than 40 mV (negative or positive) are known to have good stability in water.<sup>72</sup> Thus, polar-solvent-dispersible (more specifically, water-dispersible) GPN was generated with treatment of NMMO<sub>m</sub>.

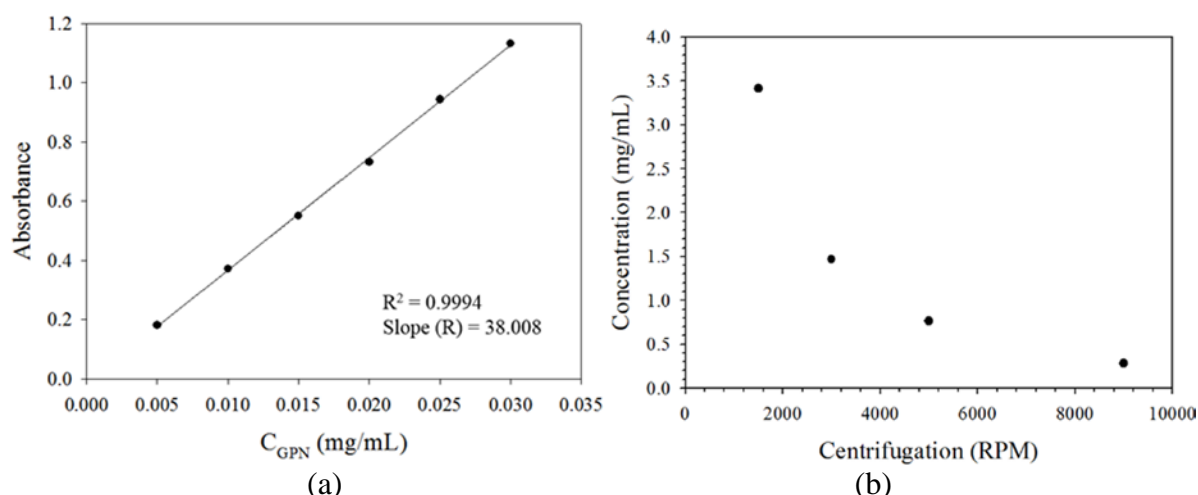
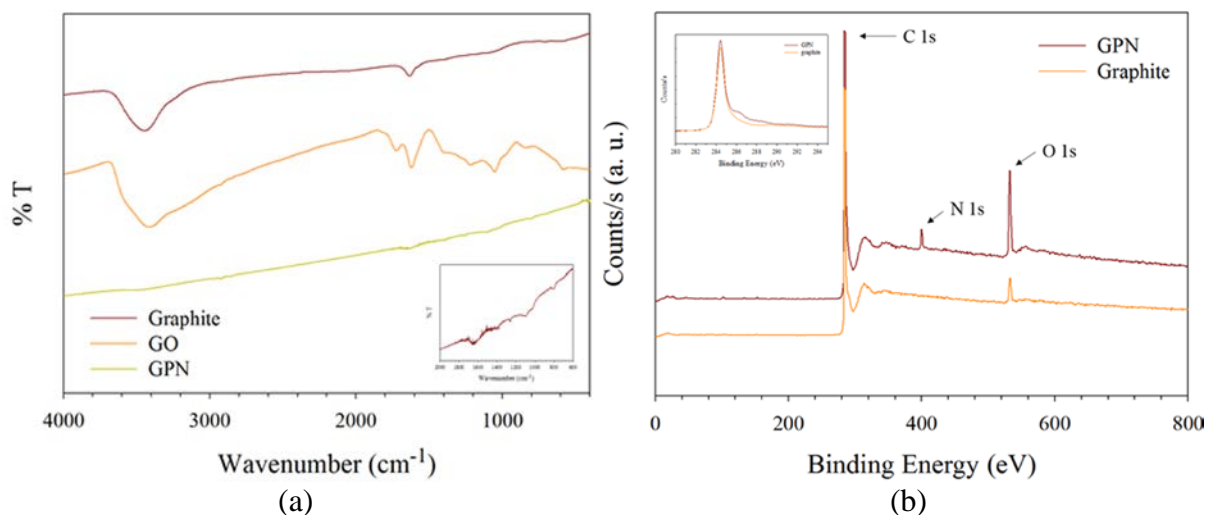


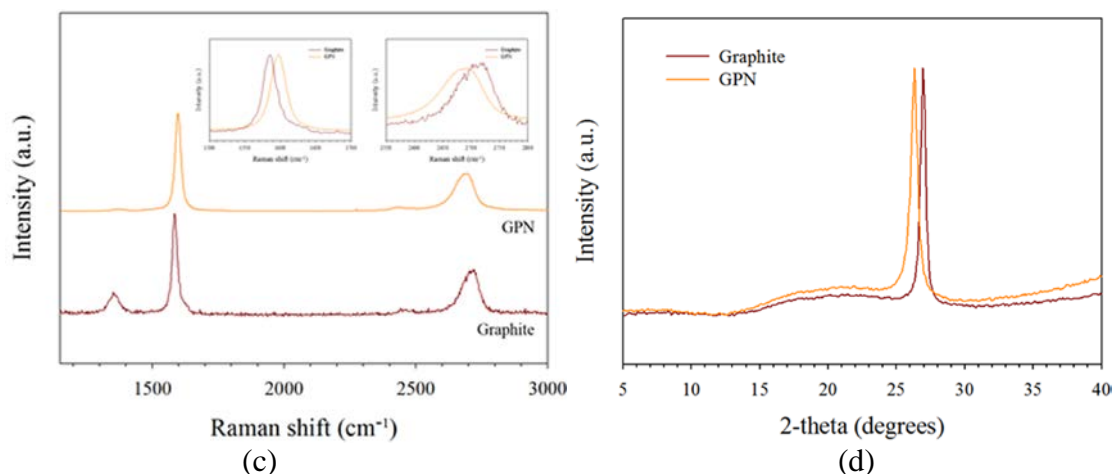
**Figure 5.** (a) UV-Vis absorbance of the aqueous GPN solution at 660 nm as a function of  $C_{\text{GPN}}$  immediately after sonication for 2 h, (b) the measured concentration from UV-Vis spectroscopy after centrifugation of the 5 mg/mL GPN solution for 10 min as a function of rpm; the data at 1,500 and 3,000 rpm were obtained from  $\times 10$  dilution with water after centrifugation.

The measurement of the amount of dispersible GPN in water is important. UV-Vis spectroscopy is commonly used to evaluate the amount of dispersible GPN in water. Coleman et al. studied the dispersion of NMP-treated graphene in NMP with centrifugation.<sup>[73]</sup> UV-Vis

spectroscopy in the range of 0.005 to 0.03 mg/mL was performed to obtain a calibration curve. Figure 5a shows the intensity at 660 nm as a function of  $C_{\text{GPN}}$ , representing a calibration curve. The straight line was obtained with good linearity ( $R^2=0.9994$ ). The slope gives an absorption coefficient,  $\alpha$ , of 38.01 mL/mg/cm in the Lambert-Beer equation. This value is quite close to the reported value (36.2 mL/mg/cm) of NMP-treated graphene in NMP studied by Coleman et al.<sup>[73-75]</sup> The kinetics of the settlement of the dispersed graphene is one of the important considerations for disperse graphene from GPN powders because the settlement of graphene is dependent on the sizes (or number of stacks) of graphene. Centrifugation can accelerate its settlement, and the rpm can control the kinetics of the settlement. To evaluate the settlement of the dispersed GPN in water, centrifugation of the concentrated GPN solution (5 mg/mL) was performed at different rpms up to 9000 rpm (the highest level in the used centrifuge). Figure 5b shows the measured concentration of the aqueous GPN after centrifugation as a function of rpm. The concentration decreases exponentially as the centrifugation speed increases. The initial concentrated aqueous GPN solution (5 mg/mL) after sonication for 2 h may contain graphene sheets with a large distribution in the number of stacks in graphene. Many-stacked graphene will be settled at low rpm and little-stacked graphene will be settled at high rpm such that the amount of the settlement increases with increasing rpm of the centrifugation. The  $C_{\text{GPN}}$  values were 3.415, 1.468, 0.766, and 0.284 mg/mL after centrifugation at 1,500, 3,000, 5,000, and 9,000 rpm, respectively. Shulin et al. reported dispersion concentrations of 0.21 and 0.03 mg/mL in a water/acetone mixture from a water/acetone mixture-treated graphene after sonication for 12 h in a sonic bath with centrifugation at 500 and 4,000 rpm, respectively.<sup>[76]</sup> Coleman et al. reported dispersion concentrations of 0.1 and 0.05 mg/mL from NMP-treated graphene in NMP after sonication for 168 h in a sonic bath with centrifugation at 500 and 4000 rpm, respectively.<sup>[77]</sup> Thus, GPN can be more dispersible in water than NMP-treated graphene in NMP.

### 3-3. Structures of GPN:

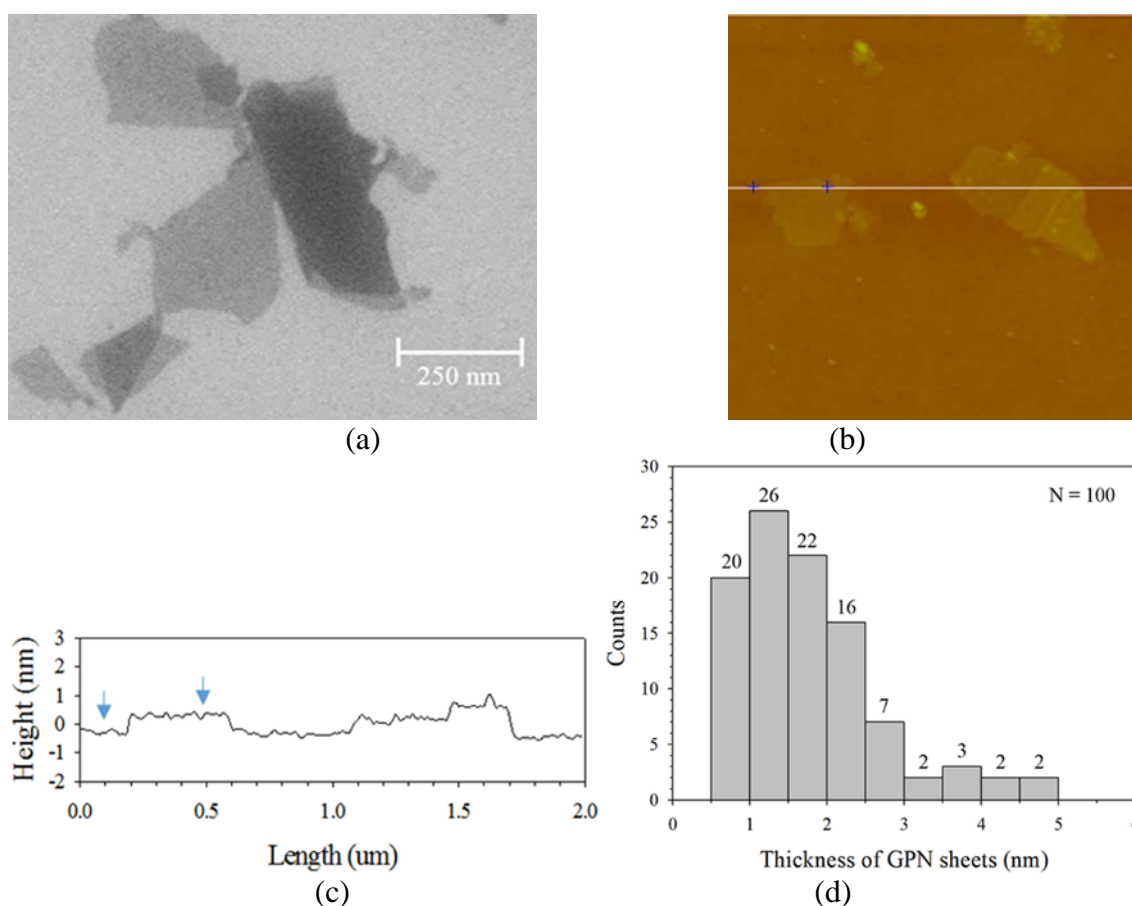




**Figure 6.** (a) FT-IR (inset: enlarged GPN spectrum below 2,000  $\text{cm}^{-1}$ ), (b) XPS (inset: enlarged C1s peak), (c) Raman spectra (inset: enlarged G and 2D peaks), and (d) WAXS patterns of the GPN and graphite samples; the GPN sample for Raman spectroscopy was prepared by spray-coating on the silicon wafer and the monolayer (or a few layers) of the GPN sample was confirmed by AFM.

The structure of GPN was analyzed by FT-IR, XPS, and Raman spectroscopies, as shown in Figure 6. The FT-IR spectrum of the GPN powders (Figure 6a) shows no discernible bands, suggesting that the GPN produced contained almost no functional groups as well as manifesting a complete graphene structure. However, the enlarged spectrum shows several small peaks which may be due to the small amounts of the remaining NMMO<sub>m</sub>. Although the detail study is necessary for assigning the peaks, we found that the N-O and C-N stretching bands at 1,261, and 1,096  $\text{cm}^{-1}$ , respectively, indicating that the small amounts of NMMO may be present in GPN. The XPS spectrum of the GPN powders (Figure 6b) exhibited a strong C 1s peak and two small N 1s and O 1s peaks. The N 1s peak was assigned to residual NMMO molecules trapped on the GPN sheet. The N, O, and C contents in the GPN were 3.46, 11.05 and 85.49 wt%, respectively. An N atom combines with two oxygens and five carbon atoms in NMMO, such that the amounts of O and C atoms from NMMO were 7.91 and 14.83 wt%, respectively, and the amounts of O and C atoms from sources other than NMMO were 3.14 and 70.66 wt%, respectively. Therefore, the C/O ratio for GPN was 22.5 after excluding the NMMO O and C atoms. Graphite itself is known to contain a small amount of oxygen atoms due to air oxidation, as shown in Figure 6b, which is consistent with other reported results.<sup>[78]</sup> Thus, the C/O ratio (22.5) would increase after exclusion of the oxygen atoms that do not participate in the structural defects. The small amount of oxygen observed in GPN indicates that the material produced had a near defect-free graphene structure. The perfect graphitic structure can be confirmed by the C1s XPS spectrum (Figure 6b inset). The graphitic carbon (C–C) and nitrogen-bonded carbon (C–N) can be observed at 284.3 and 286.2 eV, respectively. The small C–N peak is due to the remaining NMMO. However, the carbon peaks related to oxidization typically associated with GO<sup>[44,79]</sup> are not observed. These experiments again confirm that high-quality, unoxidized graphene flakes can be produced with NMMO treatment. The Raman spectrum of the GPN (and graphite) samples (Figure 6c) shows sharp D, G and 2D peaks at 1359 (1370), 1598 (1585) and 2689 (2721)  $\text{cm}^{-1}$ , respectively; the numbers in parentheses are the data for graphite. The GPN sample for Raman spectroscopy was prepared by spray-coating on the silicon wafer and the monolayer (or a few layers) of the sample was confirmed by AFM. The G peak is much higher than the D peak. The existence of the 2D peak of the GPN sample with its symmetrical shape also indicates that the structure of GPN is

close to that of graphene without defects. The presence of a D band in the graphite powders was attributed to the small Raman excitation beam size used.<sup>[19]</sup> Thus, observance of the D peak in the spectrum of the GPN may be due to the same reason. The G and 2D peaks of GPN were blue- and red-shifted compared with those of graphite powder, respectively (Figure 6c inset). The observed blue shift of the G peak and the red-shift of the 2D peak of the GPN sample compared with that of the graphite powder was attributed to the monolayer (or a few layers) of the graphene sheets.<sup>[80]</sup> Thus, the Raman spectrum of GPN was similar to that of the graphite powders, except for a slight peak shift, indicating that the structure of the produced GPN was similar to that of the graphite layer. The gallery gap in the GPN powder was examined by WAXS, as shown in Figure 6d. The WAXS pattern of the GPN powder shows a peak at  $2\theta = 26.30^\circ$  (d-spacing = 3.39 Å), which was down shifted from that of graphite ( $2\theta = 26.94^\circ$  (d-spacing = 3.31 Å)). The increased gallery gap in GPN compared to graphite was probably due to the entrapment of the remained NMMO between the GPN sheets. The FT-IR, XPS, Raman spectroscopy, and WAXS studies strongly indicate that the structure of the produced GPN is close to that of graphene without defects.



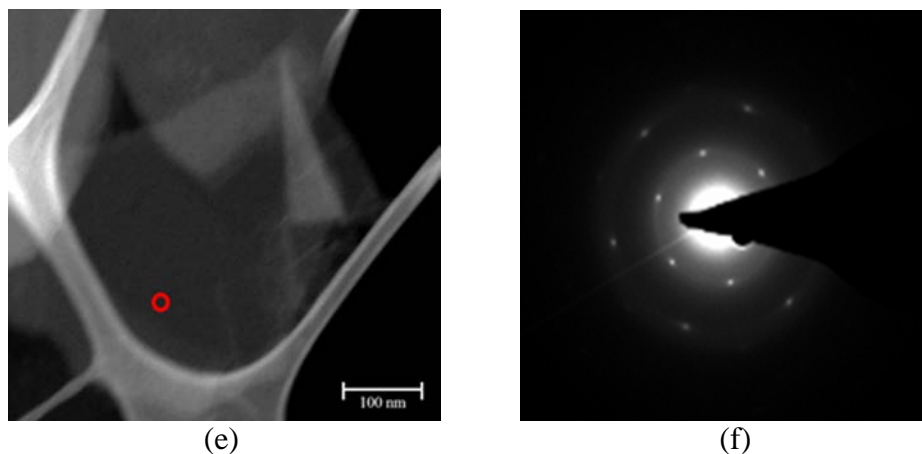


**Figure 7.** (a) SEM and (b) AFM images of the GPN on a silicon wafer; (c) height profile of the line in (b); (d) thickness distribution for one hundred arbitrary graphene measured using AFM; (e) STEM image and (f) selective area electron diffraction (SAED) pattern of the single-layered graphene in the circled area in (e).

The morphology of the GPN was studied with SEM, AFM, and STEM, as shown in Figure 7. The samples for SEM and AFM were prepared by spin coating a dilute aqueous GPN dispersion (0.001 mg/mL) on a silicon wafer. The SEM image (Figure 7a) shows the semi-transparent and darker GPNs on the silicon wafer, which represent the single-layered and overlapped layered structures, respectively. The overlapped structure may be due to restacking and/or folding of the individual single-layered sheets during the sample preparation. The AFM image (Figure 7b) reveals a single-layered structure on the silicon wafer. The layered thickness from the height profile (Figure 7c) is  $\sim 0.6$  nm, which is similar to the theoretical value of a single layer, and the length of the long axis of the GPN sheet is  $\sim 300$  nm which is a typical size for sonicated samples.<sup>[81]</sup> Figure 7d shows a representation of the observed distribution. It was found that  $> 90\%$  of the graphene sheets had three or fewer layers, and the mean layer number per flake was two. Therefore, the GPN in water was exfoliated into single layers in dispersion by simple sonication. The single-layered structure was explored in more detail using STEM with electron diffraction. The transparent sheet on the STEM grid is clearly observed in Figure 7e. The SAED pattern (Figure 7f) of the circled area in Figure 7e shows the inner (1100) diffractions and next outer (2110) diffractions with a two-dimensional hexagonal symmetry.<sup>[11]</sup> The (1100) diffractions are stronger than the (2110) diffractions. The (1100) diffractions of the single-layered graphene sheet are known to be stronger than the next (2110) diffractions, and vice-versa for the multilayers.<sup>18</sup> Most of the observed SAEDs from other samples had stronger (1100) diffractions than (2110) diffractions. Several hexagonal patterns with different intensity distribution were also observed from other samples. For example, the SAED had stronger (2110) diffractions than (1100) diffractions at the multi-layered part, and the stacking of the individual sheet was not epitaxially matched, which resulted in overlapped electron diffractions with a certain tilting angle. However, these patterns were rarely observed, indicating that most GPNs produced had the single-layered structure.

**3-4. Electrical conductivity of graphene film:** The electrical conductivity of the GPN film prepared by a filtering method was measured using a four-point probe. Its electrical conductivity was 94.7 S/cm. Samulski et al. reported electrical conductivities of 0.17, 12.5, and 61.2 S/cm from the sulfonated GO (GO-SO<sub>3</sub>H, water-soluble), graphene, and graphite, respectively.<sup>[72]</sup> This

high conductivity of 94.7 S/cm from GPN was due to the complete graphitic structure without defects, as mentioned for the FT-IR, XPS, and Raman spectroscopy results.

### 3-5. PEDOT:PSS/GPN nanocomposite:

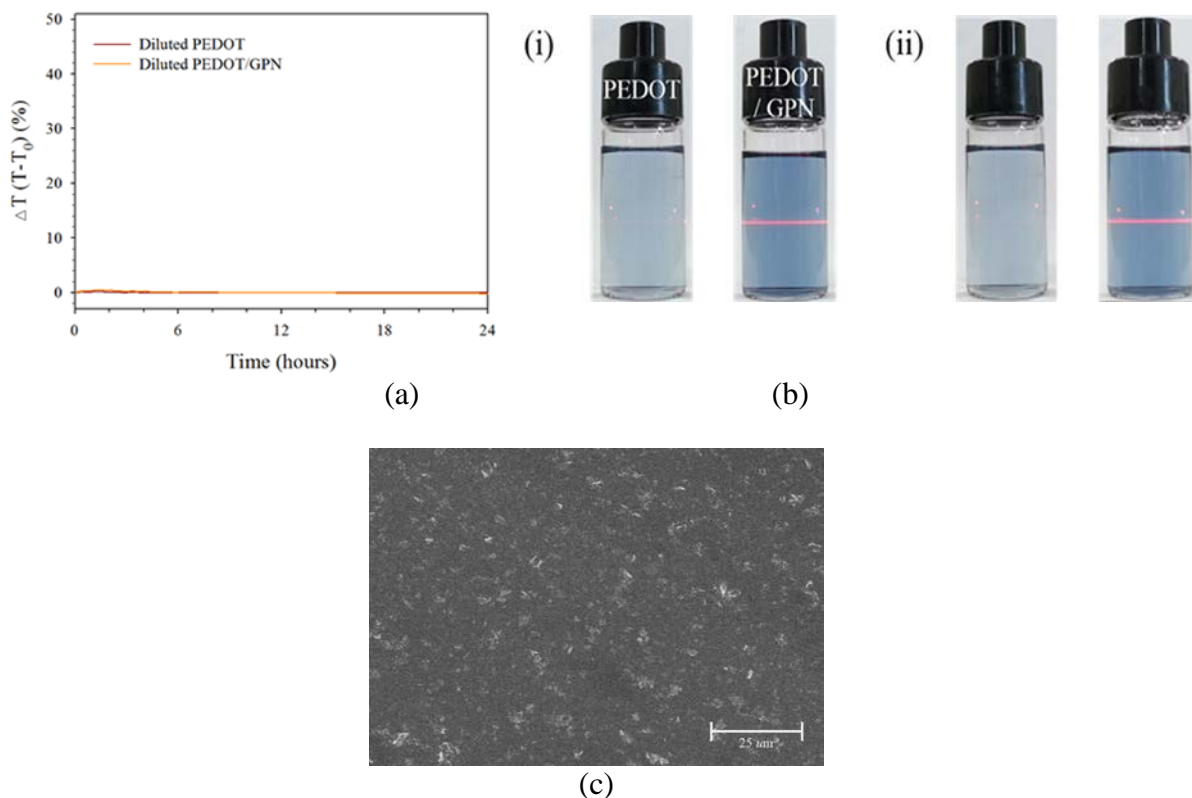


**Figure 8.** (a) Increase of the averaged transmissions ( $\Delta T = T - T_0$ ) of the PEDOT:PSS and PEDOT:PSS/GPN ( $\phi = 3$  wt%) solutions after  $\times 20$  times dilution with water during 24 h. (b) Photographs of the vials containing the PEDOT:PSS and PEDOT:PSS/GPN ( $\phi = 3$  wt%) solutions (i) immediately and (ii) 24 h after  $\times 20$  times dilution with water; the laser beams in the vials are to see the Tyndall effect. (c) SEM image of the PEDOT:PSS/GPN ( $\phi = 3$  wt%) from the sample prepared by drop-casting of the  $\times 20$  water-diluted solution on a silicon wafer and drying in an oven at 60 °C.

Water-dispersible GPN can find many applications for nanocomposites with water-soluble polymers. The aqueous PEDOT:PSS system was employed to demonstrate the improvement of the electrical properties by mixing with GPN. To study the dispersity of GPN in the aqueous PEDOT:PSS solution, the transmittance of the PEDOT:PSS/GPN solution was measured for 24 h using Turbiscan. Figure 8a shows the increase of the transmittance of PEDOT:PSS and PEDOT:PSS/GPN ( $\phi = 3$  wt%,  $\phi$  is the amount of GPN vs. the solid content of PEDOT/PSS) solutions after 20 times dilution with water; the PEDOT:PSS aqueous solution was diluted because the initial (as-received) PEDOT:PSS and PEDOT:PSS/GPN ( $\phi = 3$  wt%) aqueous solutions were too dark to measure the transmittance. The transmittances of the PEDOT:PSS and PEDOT:PSS/GPN ( $\phi = 3$  wt%) aqueous solutions do not increase within experimental errors even after 24 h. A clear laser beam from strong Tyndall scattering was observed for the PEDOT:PSS/GPN ( $\phi = 3$  wt%) aqueous solution 24 h after mixing (Figure 8b), indicating that the GPN was well dispersed in the aqueous PEDOT:PSS solution. This facile

preparation of the PEDOT:PSS/GPN solution can be used for the thin-film application by drop-coating. The drop coating on the silicon wafer as well as the bare glass was performed with 0.5 mL of the  $\times 20$  water diluted PEDOT:PSS/GPN solution and dried on a hot plate at 80°C. The prepared thin film on the silicon wafer was studied with SEM, as shown in Figure 8c. The GPN sheets extruded from the surface of the thin film are uniformly distributed on the surface of the thin film. The sizes of the extruded GPN sheets are  $\sim$  several hundred nm, which is close to the SEM and AFM results. This good dispersion of GPN in the PEDOT:PSS matrix may be due to the strong  $\pi$ - $\pi$  interactions between aromatic rings of PEDOT and the GPN.

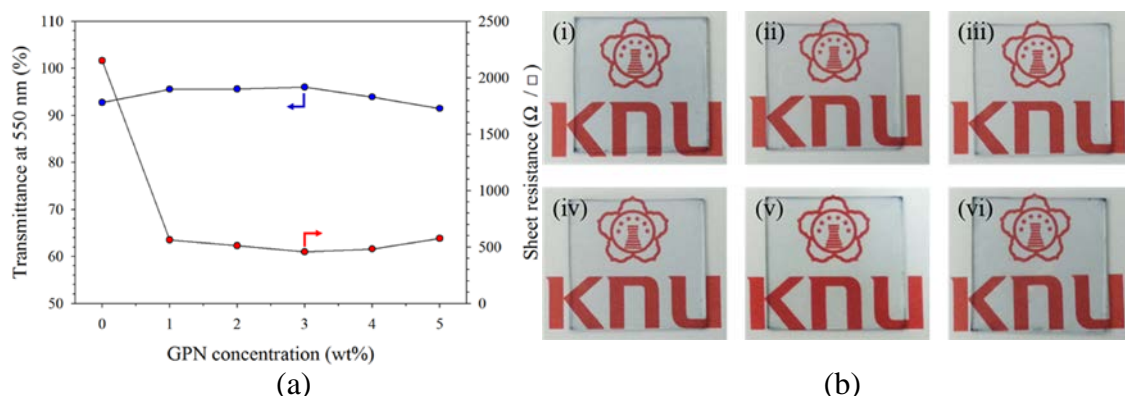


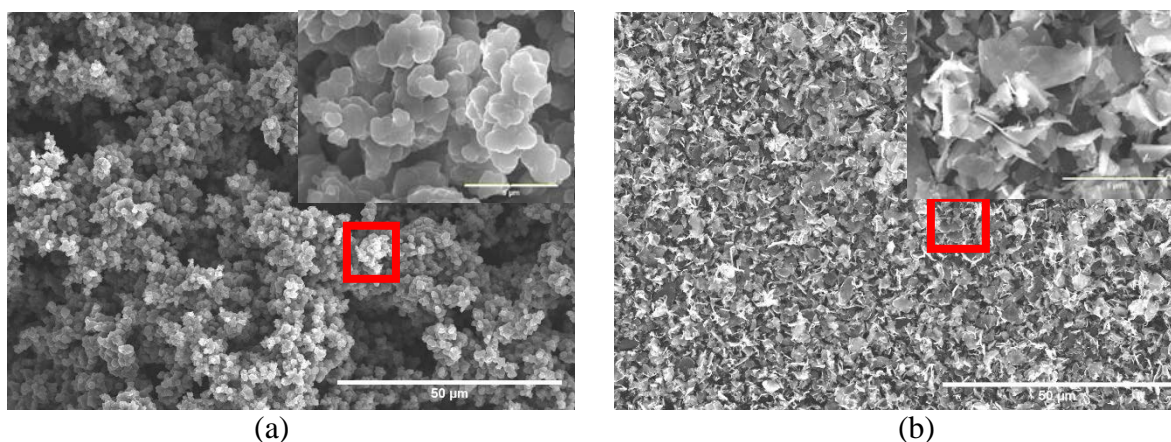
**Figure 9.** (a) (blue circle) Transmittances at 550 nm and (red circle) sheet resistances of the PEDOT:PSS/GPN nanocomposite thin films on a glass substrate as a function of  $\phi$ ; (b) images of the thin films at  $\phi =$  (i) 0, (ii) 1, (iii) 2, (iv) 3, (v) 4, and (vi) 5 wt%.

The electrical conductivity and transmittance of the spin-coated film on the glass substrate were tested. The thin film of the PEDOT:PSS was prepared with IPA mixing and ethanol treatment because the electrical conductivity of the PEDOT:PSS thin film is known to increase with IPA mixing and ethanol soaking, as discussed in the experimental section.<sup>[64,65]</sup> Figure 9a shows the transmittance at 550 nm and the sheet resistance of the spin-coated PEDOT:PSS/GPN nanocomposite thin films on the glass substrate as a function of  $\phi$  until 5 wt% at 1 wt% intervals. The thickness of the film was controlled at  $\sim 40$  nm. The spin-coated films show no aggregation on the glass substrate with good transparency, indicating that all the PEDOT:PSS/GPN aqueous solutions exhibited a good coating capability with good GPN dispersion. The sheet resistance of the pristine PEDOT:PSS ( $\phi = 0$  wt%) is 2,152  $\Omega/\square$  and decreases to 562.6, 511.8, 457.2, 482.4, and 576.3  $\Omega/\square$  at  $\phi = 1, 2, 3, 4$ , and 5 wt%, respectively. The sheet resistance of the thin film of the PEDOT:PSS/GPN decreases substantially at  $\phi = 1$  wt% (562.6  $\Omega/\square$ ) from that of the pristine PEDOT:PSS (2,152  $\Omega/\square$ ), slightly decreases with further increase of the GPN until  $\phi = 3$  wt%, and then slightly increases. The sheet resistances of all the PEDOT:PSS/GPN thin films (at  $\phi = 1, 2, 3, 4$ , and 5 wt%) are  $\sim 4$  times lower than that of the pristine PEDOT:PSS thin film. This improvement of the electrical conductivity is due to the good dispersity of GPN in the aqueous PEDOT:PSS solution and the graphitic structure of GPN without defects. The good dispersion of the GPN in the aqueous PEDOT:PSS solution may be due to the  $\pi$ - $\pi$  interactions between aromatic rings of PEDOT and graphene.<sup>[82]</sup> However, the decrease of the sheet resistance is not significant after  $\phi = 1$  wt%, and the minimum sheet resistance was observed at  $\phi = 3$  wt%. The difference in the sheet resistance between  $\phi = 1$  and 3 wt% is only 30  $\Omega/\square$ , which might be due to the overlapping and aggregation of GPN in the PEDOT:PSS matrix. However, a more detailed study is necessary to determine the exact reasons for the slight decrease of the sheet resistance after  $\phi = 1$  wt%. The PEDOT:PSS/GPN thin films

exhibit transmittances of 92.8, 95.5, 95.6, 95.9, 93.9, and 91.5 % at  $\phi = 0, 1, 2, 3, 4$  and 5 wt%, respectively. Figure 9b presents their transparent photo images on the KNU letters. The transmittances of the PEDOT:PSS thin films are not affected much at  $\sim 94 \pm 2$  % by the addition of GPN. The transmittance of the PEDOT:PSS thin films even increases with the addition of GPN until  $\phi = 3$  wt%. Several reasons, such as the matched refractive indices between GPN and PEDOT:PSS,<sup>[83]</sup> the decreased size of the PEDOT by sonication,<sup>[65]</sup> and/or the compensation of the blue color of PEDOT by the black color of GPN,<sup>[84]</sup> may explain the decrease of the transmittance. The transmittance decreases with further addition of GPN at  $\phi > 3$  wt% most likely because of the aggregation of the GPN in the PEDOT:PSS matrix. However, the transmission levels are still high enough for transparent electrode applications. In this study, we observed a fourfold increase in the electrical conductivity of the PEDOT:PSS with the addition of 1 wt% GPN without deterioration of the transparency (and even a small improvement in the transparency).

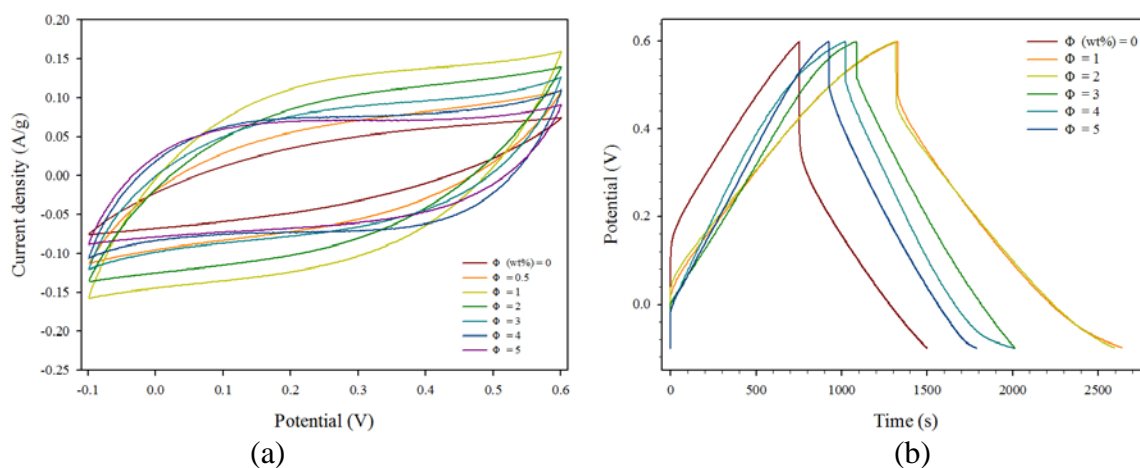
### 3-8. Preparation of PPy/GPN nanocomposites

Conducting polymers such as polyaniline, polypyrrole (PPy), and polythiophene have been studied extensively in the last few decades because of their good electrical properties, high specific capacity, easy processability, and light weight. Amongst these, PPy is one of the most promising electrode materials for pseudocapacitors because of its high electrical conductivity in the doped state, high specific capacitance, good environmental stability, low cost, and facile synthesis.<sup>[86-91]</sup> Moreover, the mechanical flexibility of PPy is an additional advantage over other conductive polymers because it is able to meet the rising demand for flexible supercapacitors.<sup>[92]</sup> However, PPy is usually mechanically weak and insulating in its neutral state, which hinders some of its applications. It also undergoes swelling, shrinkage, and cracking or breaking, which induces gradual deterioration of the conductivity and causes volumetric changes, leading to poor charge–discharge cycle stability.<sup>[93]</sup> One way to overcome this drawback is to support PPy on a carbon-based material.<sup>[94]</sup> Recent research has mainly focused on carbon-nanostructured materials such as carbon nanotubes (CNTs) and graphene to solve this poor charge–discharge cycle stability.<sup>[95,96]</sup> One advantage of incorporating water-dispersible graphene in PPy/graphene nanocomposites is that PPy can be polymerized in situ in water with water-dispersible graphene. Bose et al. successfully prepared PPy/reduced graphene oxide (rGO) nanocomposites by in situ polymerization of graphene oxide (GO) and pyrrole monomer followed by chemical reduction using hydrazine monohydrate.<sup>[97]</sup> The nanocomposite exhibited good improvement in thermal stability as well as electrical conductivity, with a conductivity of approximately 8 S/cm, which is  $\sim 40$  times greater than PPy without the graphene.<sup>[97]</sup> Han and coworkers demonstrated in situ polymerization by ammonium persulfate and subsequent reduction by  $\text{NaBH}_4$  to synthesize PPy/rGO nanocomposites.<sup>[98]</sup> The increased capacitance of 180 F/g compared with that of pristine GO (11 F/g) and PPy (112 F/g) could be ascribed to the synergistic effect between GO and PPy. Liu et al. synthesized nanocomposite films of sulfonated graphene and PPy by electrochemical deposition from aqueous solutions containing pyrrole monomer, sulfonated graphene sheets, and dodecylbenzene sulfonic acid.<sup>23</sup> The PPy/sulfonated graphene nanocomposite exhibited improved conductivity, electrochemical stability, and rate performance. All the PPy nanocomposite systems studied until now used GO, or chemically (or electrochemically) reduced GO, or chemically functionalized GO (e.g. sulfonated graphene) in aqueous solutions.<sup>24</sup> However, direct exfoliated graphene has not been used for PPy/graphene nanocomposite systems mostly because it cannot be dispersed in aqueous solutions, although defect-free graphene would be a perfect candidate for application to a PPy/graphene nanocomposite system.



**Figure 10.** SEM images of the (a) PPy and (b) PPy/eGPNc (1 wt%) powders with the insets showing the magnified image of the box.

Figure 10 shows the SEM images of pure PPy and PPy/eGPNc (1 wt%) with the insets showing the enlarged images. The SEM image of the pure PPy shows irregular sphere-like particles with a size of  $\sim 1 \mu\text{m}$  and the PPy/eGPNc (1 wt%) exhibits a plate-like morphology, indicating that a coating of PPy is formed on the eGPNc sheet, which is completely different from that of PPy. The image of the PPy is similar to that previously reported.<sup>[101]</sup> During in situ polymerization of PPy with eGPNc in water, pyrrole monomers are known to have contacts on the graphene sheet by  $\pi$ - $\pi$  interactions and are polymerized on the graphene surface.<sup>[101]</sup> Similar morphology was reported with PPy/rGO nanocomposite systems.<sup>35</sup> Thus, the well dispersed graphene in the PPy/graphene nanocomposite was produced by a simple in situ polymerization of PPy in the presence of water-dispersible graphene in water without any further reductions used for PPy/GO nanocomposites.



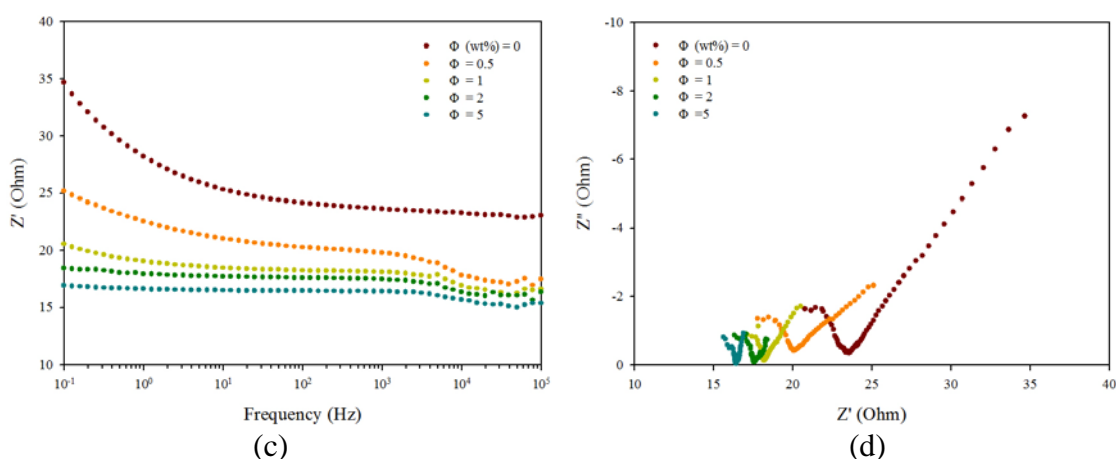


**Figure 11.** (a) Cyclic voltammetry (CV) and (b) galvanostatic charge/discharge (GCD) curves of the PPy/eGPNC nanocomposites at different eGPNC content ( $\phi$ s) over a potential range of - 0.1 to 0.6 V (vs. SCE) at a scan rate of 1 mV/s (CV) and 0.1 A/g (GCD); (c) impedance and (d) Nyquist plot of PPy/eGPNC nanocomposites at different eGPNC content ( $\phi$ s) with an amplitude of 10 mV.

The electrochemical performance of the PPy/eGPNC nanocomposites as electrode materials for supercapacitors was tested by cyclic voltammetry (CV) and galvanostatic charge–discharge (GCD) techniques in a three-electrode system. Figure 11a exhibits the CV curves of the PPy/eGPNC nanocomposites at different eGPNC content ( $\phi$ s) over a potential range of - 0.1 to 0.6 V (vs. saturated calomel reference electrode (SCE)) at a scan rate of 1 mV/s. The shapes of all CV curves show a symmetric current-potential characteristic. In addition, it was observed that there were no clear redox peaks over the potential range of -0.1 to 0.6 V. The capacitances of the PPy/eGPNC nanocomposites calculated from the area of the closed loop are 122.8, 278.6, 208.6, 178.8, 162.7, and 144.9 F/g at  $\phi = 0, 1, 2, 3, 4$ , and 5 wt%, respectively with a maximum at  $\phi = 1$  wt%. Figure 11b shows the galvanostatic charge–discharge (GCD) curves of PPy/eGPNC nanocomposites at different  $\phi$ s over a potential range of -0.1 to 0.6 V (vs. SCE) at a current of 0.1 A/g. The current-resistant (IR) drops of the PPy/eGPNC nanocomposites at  $\phi = 0, 1, 2, 3, 4$ , and 5 wt% are 0.21, 0.13, 0.14, 0.09, 0.10, and 0.10 V, respectively. A high IR drop, which has been reported, is observed for the pure PPy and decreases as the  $\phi$  increases.<sup>[102]</sup> This decrease in the IR-drop of the PPy/eGPNC nanocomposites (compared to that of the pure PPy) reflects an increase in the conductivity because of the incorporated graphene, and contribute to an improvement in the symmetry between the charge and discharge curves. The IR drop is usually caused by the overall internal resistance of the devices, and the low IR drop is be associated with a moderate amount of electroactive materials and the contact between the electroactive materials and electrode substrate. It should be pointed out that low internal resistance is of great importance in energy-storing devices, as less energy will be wasted in producing unwanted heat during the charging/discharging processes.<sup>[103]</sup> The specific capacitance of the electrode using GCD can be calculated according to the following equation  $C = (I \times \Delta t) / (m \times \Delta V)$  where  $I$  is the current,  $\Delta V$  is the potential window,  $\Delta t$  is the discharge time, and  $m$  is the mass of active material in a single electrode. The specific capacitances at  $\phi = 0, 1, 2, 3, 4$ , and 5 wt% are 107.6, 189.3, 182.3, 155.0, 145.7, and 132 F/g, respectively. The inclusion of eGPNC results in an increase in the characteristic charge/discharge times with a maximum at  $\phi = 1$  wt%, similar to the results obtained from the CV curves, which reflects an improvement in capacitance.

Figures 11c and d show the impedance and Nyquist plots of PPy/eGPNC nanocomposites at different  $\phi$ s with an amplitude of 10 mV, respectively. Nyquist plots consist of two sections: a semi-circle at the high frequency range (low  $Z'$ ) and a linear slope at the low frequency range (high  $Z'$ ). At the high frequency range, a large semi-circle reflects the high charge transfer resistance attributed to the poor electrical conductivity of the samples. PPy/eGPNC nanocomposites have smaller semi-circles as  $\phi$  increases. At the low frequency range, the shorter straight line indicates more ideal capacitor. Because of the frequency dependence of ion diffusion/transport in the electrolyte, the Warburg resistance is represented by the 45° slope line. The larger Warburg region (long straight line) reflects a longer diffusion path length of the ions and increases obstruction to ion movement. From the Nyquist plot, it is observed that PPy/eGPNC displays a much shorter ion diffusion path length compared to PPy, which is consistent with the results obtained from the GCD analysis.

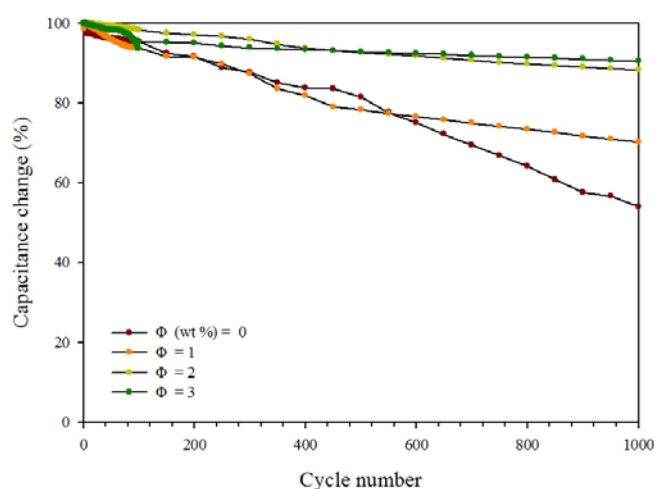


**Figure 12.** Capacitance change of the PPy/eGPNC nanocomposites at different eGPNC content ( $\phi$ s) over a potential range of - 0.1 to 0.6 V (vs. SCE) at a scan rate of 50 mV/s (CV).

The stabilities of the capacitances of the PPy/eGPNC nanocomposites were studied after 1000 CV cycles. Figure 12 shows the capacitance change of the PPy/eGPNC nanocomposites at different  $\phi$ s over a potential range of - 0.1 to 0.6 V (vs. SCE) at a scan rate of 50 mV/s (CV). The capacitance of the PPy/eGPNC nanocomposite decreases continuously as the cycle number increases. After 1000 cycles, the capacitance decreases by 53.98, 70.21, 88.29, and 91.03 % at  $\phi = 0, 1, 2$ , and 3 wt%, respectively. The stability of the capacitance of PPy is increased from 53.98 to 91% by loading 3 wt% eGPNC. The capacitance decreases as  $\phi$  increases, although the decrease in the capacitance is almost saturated at  $\phi = 1$  wt%. This improvement demonstrates that eGPNC is effective in elevating the stability of the capacitance of PPy by incorporating small amounts of eGPNC in the nanocomposite.

#### <references>

1. M. Segal, Nature Nanotech., 2009, 4, 612-614.
2. C. Lee, X. D. Wei, S. W. Kysar and J. Hone, Science, 2008, 321, 385-388.
3. A. A. Balandin, S. Ghosh, W. Z. Bao, I. Calizo, D. Teweldebrhan, F. Miao and C. N. Lau, NanoLett., 2008, 8, 902-907.
4. N. Behabtu, J. R. Lomeda, M. J. Green, A. L. Higginbotham, A. Sinitskii, D. V. Kosynkin, D. Tsentalovich, A. N. G. Parra-Vasquez, J. Schmidt, E. Kesselman, Y. Cohen, Y. Talmon, J. M.

- Tour and M. Pasquali, *Nature Nanotech.*, 2010, 5, 406-411.
5. A. K. Geim, S. V. Morozov, D. Jiang, Y. Zhang, S. V. Dubonos, I. V. Grigorieva and A. A. Firsov, *Science*, 2004, 306, 666-669.
  6. D. C. Wei, Y. Q. Liu, Y. Wang, H. L. Zhang, L. P. Huang and G. Yu, *NanoLett.*, 2009, 9, 1752-1758.
  7. J. H. Park, W. C. Mitchel, L. Grazulis, K. Eyink, H. E. Smith and J. E. Hoelscher, *Carbon*, 2011, 49, 631-635.
  8. P. W. Sutter, P. M. Albrecht and E. A. Sutter, *Appl. Phys. Lett.*, 2010, 97, 213101-213103.
  9. R. Hao, W. Qian, L. H. Zhang and Y. L. Hou, *Chem. Commun.*, 2008, 44, 6576-6578.
  10. W. Qian, R. Hao, Y. L. Hou, Y. Tian, C. M. Shen, H. J. Gao and X. L. Liang, *Nano Res.*, 2009, 2, 706-712.
  11. M. J. McAllister, J. L. Li, D. H. Adamson, H. C. Schniepp, A. A. Abdala, J. Liu, M. Herrera-Alonso, D. L. Milius, R. Car, R. K. Prud'homme and I. A. Aksay, *Chem. Mater.*, 2007, 19, 4396-4404.
  12. S. Stankovich, D. A. Dikin, R. D. Piner, K. A. Kohlhaas, A. Kleinhammes, Y. Jia, Y. Wu, S. T. Nguyen and R. S. Ruoff, *Carbon*, 2007, 45, 1558-1565.
  13. X. Cui, C. Z. Zhang, R. Hao and Y. L. Hou, *Nanoscale*, 2011, 3, 2118-2126.
  14. W. S. Hummers and R. E. Offeman, *J. Am. Chem. Soc.*, 1958, 80, 1339.
  15. H. C. Schniepp, K. N. Kudin, J.-L. Li, R. K. Prud'homme, R. Car, D. A. Saville and I. A. Aksay, *ACS Nano*, 2008, 2, 2577-2584.
  16. Q. Su, S. Pang, V. Alijani, C. Li, X. Feng and K. Mullen, *Adv. Mater.*, 2009, 21, 3191-3195.
  17. S. Pang, H. N. Tsao, X. Feng and K. Mullen, *Adv. Mater.*, 2009, 21, 3488-3491.
  18. Y. Hernandez, V. Nicolosi, M. Lotya, F. M. Blighe, Z. Y. Sun, S. De, I. T. McGovern, B. Holland, M. Byrne, Y. K. Gun'ko, J. J. Boland, P. Niraj, G. Duesberg, S. Krishnamurthy, R. Goodhue, J. Hutchison, V. Scardaci, A. C. Ferrari and J. N. Coleman, *Nat. Nanotechnol.*, 2008, 3, 563-568.
  19. M. Lotya, Y. Hernandez, P. J. King, R. J. Smith, V. Nicolosi, L. S. Karlsson, F. M. Blighe, S. De, Z. Wang, I. T. McGovern, G. S. Duesberg and J. N. Coleman, *J. Am. Chem. Soc.*, 2009, 131, 3611-3620.
  20. J. N. Coleman, *Adv. Funct. Mater.*, 2009, 19, 3680-3695.
  21. J. N. Coleman, *Acc. Chem. Res.*, 2013, 46, 14-22.
  22. X. Y. Zhang, A. C. Coleman, N. Katsonis, W. R. Browne, B. J. van Wees and B. L. Fering, *Chem. Commun.*, 2010, 46, 7539-7541.
  22. A. B. Bourlinos, V. Georgakilas, R. Zboril, T. A. Steriotis and A. K. Stubos, *Small*, 2009, 5, 1841-1845.
  23. M. Inagaki, Elsevier, Amsterdam, 2000, (2) M. Inagaki, *J. Mater. Res.*, 1989, 4, 1560-1568.
  24. Y. Sun, S. R. Wilson and D. I. Schuster, *J. Am. Chem. Soc.*, 2001, 123, 5348-5349.
  25. F. Zhang and Y. Fang, *J. Phys. Chem. B*, 2006, 110, 9022-9026.
  26. W. Du, X. Jiang and L. Zhu, *J. Mater. Chem. A*, 2013, 1, 10592-10606.
  27. X. Q. Wang, P. F. Fulvio, G. A. Baker, G. M. Veith, R. R. Unocic, S. M. Mahurin, M. F. Chi and S. Dai, *Chem. Commun.*, 2010, 46, 4487-4489.
  28. D. Nuvoli, L. Valentini, V. Alzari, S. Scognamillo, S. B. Bon, M. Piccinini, J. Illescas and A. Mariani, *J. Mater. Chem.*, 2011, 21, 3428-3431.
  29. Y. Hernandez, M. Lotya, D. Rickard, S. D. Bergin and J. N. Coleman, *Langmuir*, 2010, 26, 3208-3213.
  30. A. O'Neill, U. Khan, P. N. Nirmalraj, J. Boland and J. N. Coleman, *J. Phys. Chem. C*, 2011, 115, 5422-5428.
  31. E.-Y. Choi, W. S. Choi, Y. B. Lee and Y. -Y. Noh, *Nanotechnology*, 2011, 22, 365601.

32. S. Vadukumpully, J. Paul and S. Valiyaveetil, *Carbon*, 2009, 47, 3288-3294.
33. R. J. Smith, M. Lotya and J. N. Coleman, *New J. Phys.*, 2010, 12, 125008.
34. M. Lotya, P. J. King, U. Khan, S. De and J. N. Coleman, *ACS Nano*, 2010, 4, 3155-3162.
35. L. Guardia, M. J. Fern'andez-Merino, J. I. Paredes, P. Sol'is-Fern'andez, S. Villar-Rodil, A. Mart'inez-Alonso and J. M. D. Tasc'on, *Carbon*, 2011, 49, 1653-1662.
36. A. B. Bourlinos, V. Georgakilas, R. Zboril, T. A. Steriotis, A. K. Stubos, C. Trapalis, *Solid State Communications*, 2009, 149, 2172-2176.
37. Y. Xu , H. Bai , G. Lu , C. Li and G. Shi, *J. Am. Chem. Soc.*, 2008, 130, 5856-5857.
38. M. Zhang, R. R. Parajuli, D. Mastrogiovanni, B. Dai, P. Lo, W. Cheung, R. Brukh, P. L. Chiu, T. Zhou, Z. Liu, E. Garfunkel and H. He, *Small*, 2010, 6, 1100-1107.
39. J. Guo, L. Ren, R. Wang, C. Zhang, Y. Yang and T. Liu, *Composites Part B: Engineering*, 2011, 42, 2130-2135.
40. G. S. Bang, H.-M. So, M. J. Lee and C. W. Ahn, *J. Mater. Chem.*, 2012, 22, 4806-4810.
41. A. B. Bourlinos, V. Georgakilas, R. Zboril, T. A. Steriotis, A. K. Stubos, C. Trapalis, *Solid State Communications*, 2009, 149, 2172-2176.
42. C. Shan, H. Yang, D. Han, Q. Zhang, A. Ivaska and L. Niu, *Langmuir*, 2009, 25, 12030-12033.
43. H. Bai, Y. Xu, L. Zhao, C. Li and G. Shi, *Chem. Commun.*, 2009, 13, 1667-1669.
44. D. Li, M. B. M'uller, S. Gilje, R. B. Kaner and G. G. Wallace, *Nature Nanotechnology*, 2008, 3, 101-105.
45. J. Gassan and A. K. Bledzki, *J. Appl. Polym. Sci.* 1999, 71, 623-629.
46. C. H. Kuo, and C. K. Lee, *Bioresource Technology*, 2009, 100, 866-871.
47. H.-P. Fink, P. Weigel, H. J. Purz and J. Ganster, *Prog. Polym. Sci.*, 2001, 26, 1473-1524.
48. T. Rosenau, A. Potthast, H. Sixta and P. Kosma, *Prog. Polym. Sci.*, 2001, 26, 1763-1837.
49. H. Chanzy, E. Maia and S. Perez, *Acta Cryst. B*, 1982, 38, 852-855.
50. C. Michels and B. Kosan, *Lenzinger Berichte* 2005, 84, 62-70.
51. L. X. Benedict, N. G. Chopra, M. L. Cohen, A. Zettl, S. G. Louie and V. H. Crespi, *Chem. Phys. Lett.*, 1998, 286, 490-496.
52. L. A. Girifalco and R. J. Good, *J. Phys. Chem.*, 1957, 61, 904-909.
53. M. Hodak and L. A. Girifalco, *Chem. Phys. Lett.*, 2001, 350, 405-411.
54. R. Zacharia, H. Ulbricht and T. Hertel, *Phys. Rev. B*, 2004, 69, 155406.
55. J.-S. Yeo, J.-M. Yun, M. Kang, D. Kim, S.-H. Lee, S.-S. Kim, S.-I. Na, D.-Y. Kim, *ACS Appl. Mater. Interfaces*, 2014, 6, 19613-19620.
56. J. P. Thomas, L. Zhao, D. McGillivray, K. T. Leung, *J. Mater. Chem. A*, 2014, 2, 2383-2389.
57. Y. H. Kim, C. Sachse, M. L. Machala, C. May, *Adv. Funct. Mater.*, 2011, 21, 1076-1081.
58. J.-G. Chen, H.-Y. Wei, K.-C. Ho , *Sol. Energy Mater. Sol. Cells*, 2007, 91, 1472-1477.
59. Zhang, B.; Tan, G.; Lam, C.-S.; Yao, B.; Ho, C.-L.; Liu, L.; Xie, Z.; Wong, W.-Y.; Ding, J.; Wang, L. *Adv. Mater.*, 2012, 24, 1873-1877.
60. Zhu, Z.-T.; Mabeck J. T.; Zhu, C.; Cady N. C.; Batt, C. A.; Malliaras, G. G. *Chem. Commun.*, 2004, 1556-1557.
61. Kus, M.; Okur, S. *Sens. Act. B*, 2009, 143, 177-181.
62. B. Gupta et al *Materials Chemistry and Physics* 147 (2014) 867-877.
63. X. Wu et al. *J. Mater. Chem. C*, 2014, 2, 4044-4050.
64. H. Park, Y. Shi and J. Kong, *Nanoscale*, 2013, 5, 8934-8939.
65. D. Alemu, H. -Y. Wei, K. -C. Ho and C. -W. Chu, *Energy Environ. Sci.*, 2012, 5, 9662-9671.
66. J. Seo, S. Park, Y. C. Kim, N. J. Jeon, J. H. Noh, S. C. Yoon and S. I. Seok, *Energy Environ. Sci.*, 2014, 7, 2642-2646.

67. T. –W. Lee and Y. Chung, *Adv. Funct. Mater.*, 2008, 18, 2246-2252.
68. D. Eichinger, C. Lotz and A. G. Lenring, *Lenzinger Berichte*, 1996, 75, 69-72.
69. R. L. D. Whitby, A. Korobeinyk, V. M. Gun'ko, R. Busquets, A. B. Cundy, K. László, J. Skubiszewska-Zieba, R. Leboda, E. Tombacz, I. Y. Toth, K. Kovacs and S. V. Mikhalovsky, *Chem. Commun.*, 2011, 47, 9645-9647.
70. C. Chen, W. Kong, H. –M. Duan and Jun Zhang, *Phys. Chem. Chem. Phys.*, 2014, 16, 12858-12864.
71. N. B. Godfrey, *Chemtech*, 1972, 6, 359-363.
72. Y. Si and E. T. Samulski, *Nano Lett.*, 2008, 8, 1679-1682.
73. U. Khan, A. O'Neill, M. Lotya, S. De and J. N. Coleman, *Small*, 2010, 6, 864-871.
74. P. May, U. Khan, J. M. Hughes and J. N. Coleman, *J. Phys. Chem. C*, 2012, 116, 11393-11400.
75. U. Khan, H. Porwal, A. O'Neill, K. Nawaz, P. May and J. N. Coleman, *Langmuir*, 2011, 27, 9077-9082.
76. M. Yi, Z. Shen, X. Zhang and S. Ma, *J. Phys. D: Appl. Phys.*, 2013, 46, 025301.
77. U. Khan, A. O'Neill, H. Porwal, P. May, K. Nawaz and J. N. Coleman, *Carbon*, 2012, 50, 470-475.
78. Y. Wen, K. He, Y. Zhu, F. Han, Y. Xu, I. Matsuda, Y. Ishii, J. Cumings and C. Wang, *Nature Communications*, 2014, 5, 4033.
79. G. Eda, G. Fanchini, and M. Chhowalla, *Nature Nanotech.*, 2008, 3, 270-274.
80. D. Yoon, H. Moon and H. Cheong, *J. Korean Phys. Soc.*, 2009, 55, 1299-1303.
81. H. C. Schniepp, J. –L. Li, M. J. McAllister, H. Sai, M. Herrera-Alonso, D. H. Adamson, R. K. Prud'homme, R. Car, D. A. Saville and I. A. Aksay, *J. Phys. Chem. B*, 2006, 110, 8535-8539.
82. G. H. Kim, D. H. Hwang and S. I. Woo, *Phys. Chem. Chem. Phys.*, 2012, 14, 3530-3536.
83. J. Franklin and Z. Y. Wang, *Chem. Mater.*, 2002, 14, 4487-4489.
84. D. –H. Kim and S. –Y. Park, *Polymer*, 2014, 55, 2928-2935.
85. D. H. Kim, L. S. Tan and S. Y. Park, Preparation of water-dispersible graphene using N-methylmorpholine N-oxide monohydrate and its application for the preparation of nanocomposites using PEDOT *J. Mater. Chem. C*, 2015, 3, 7105-7117.
86. Zhang L. L., Zhao S., Tian X. N. and Zhao X. S., Layered graphene oxide nanostructures with sandwiched conducting polymers as supercapacitor electrodes *Langmuir*, 2010, 26, 17624–17628.
87. Attia N. F., Lee S. M., Kim H. J. and Geckeler K. E., Nanoporous polypyrrole: Preparation and hydrogen storage properties *International Journal of Energy Research*. 2014, 38, 466–476.
88. Wu T. M. and Lin S. H., Synthesis, characterization, and electrical properties of polypyrrole/multiwalled carbon nanotube composites *J. Polym. Sci. Polym. Chem.*, 2006, 44, 6449–6457.
89. Y. Q. Han, X. T. Qing, S. J. Ye and Y. Lu, Conducting polypyrrole with nanoscale hierarchical structure *Synth. Met.*, 2010, 160, 1159-1166.
90. Lim Y. S., Tan Y. P., Lim H. N., Huang N. M. and Tan W. T., Preparation and characterization of polypyrrole/graphene nanocomposite films and their electrochemical performance *Journal of Polymer Research*, 2013, 20, 1-10.
91. Cvetko B. F., Brungs M. P., Burford R. P. and Skyllas-Kazacos M., Structure, strength and electrical performance of conducting polypyrroles *Journal of Materials Science*, 1988, 23, 2102-2106.
92. Snook G. A., Kao P. and Best A. S., Conducting-polymer based supercapacitor devices and electrodes. *Journal of Power Sources*, 2011, 196, 1-12.
93. A. Faye, G. Dione, M. M. Dieng, J. J. Aaron, H. Cachet and C. Cachet, Usefulness of a

nanocomposite electrode with a carbon surface modified by electrosynthesized polypyrrole for supercapacitor applications J. Appl. Electrochem., 2010, 40, 1925–1931.

94. J. P. Wang, Y. L. Xu, J. Wang, X. F. Du, F. Xiao and J. B. Li, High charge/discharge rate polypyrrole films prepared by pulse current polymerization Synth. Met., 2010, 160, 1826–1831.

95. H. K. Jeong, M. Jin, E. J. Ra, K. Y. Sheem, G. H. Han, S. Arepalli and Y. H. Lee, Enhanced electric double layer capacitance of graphite oxide intercalated by poly (sodium 4-styrenesulfonate) with high cycle stability ACS Nano, 2010, 4, 1162–1166.

96. Z. Chen, V. Augustyn, J. Wen, Y. W. Zhang, M. Q. Shen, B. Dunn and Y. F. Lu, High-performance supercapacitors based on intertwined CNT/V<sub>2</sub>O<sub>5</sub> nanowire nanocomposites Adv. Mater., 2011, 23, 791–795.

97. Bose S., Kuila T., Uddin M. E., Kim N. H., Lau T. and Lee J. H., In-situ synthesis and characterization of electrically conductive polypyrrole/graphene nanocomposites Polymer, 2010, 51, 5921–5928.

98. Y. Q. Han, L. A. Hao and X. G. Zhang, Preparation and electrochemical performances of graphite oxide/polypyrrole nanocomposites Synth. Met., 2010, 160, 2336–2340.

99. Liu A., Chun L., Bai H. and Shi G., Electrochemical deposition of polypyrrole/sulfonated graphene composite films J Phys. Chem. C., 2010, 114, 22783–22789.

100. J. Xu, K. Wang, S. Z. Zu, B. H. Han and Z. Wei, Hierarchical nanocomposites of polyaniline nanowire arrays on graphene oxide sheets with synergistic effect for energy storage ACS Nano, 2010, 4, 5019–5026.

101. J. Yin, R. Chang, Y. Shui and X. Zhao, Preparation and enhanced electro-responsive characteristic of reduced graphene oxide/polypyrrole composite sheet suspensions Soft Matter, 2013, 9, 7468–7478.

102. H. Zhou, G. Han, Y. Xiao, Y. Chang and H. J. Zhai, Facile preparation of polypyrrole/graphene oxide nanocomposites with large areal capacitance using electrochemical codeposition for supercapacitors Journal of Power Sources, 2014, 263, 259–267.

103. M. Jin, Y.Y. Liu, Y.L. Li, Y.Z. Chang, D.Y. Fu, H. Zhao and G.Y. Han, Preparation of the flexible polypyrrole/polypropylene composite fibrous film for electrochemical capacitor J. Appl. Polym. Sci., 2011, 122, 3415–3422.

**List of Publications and Significant Collaborations that resulted from your AOARD supported project:** In standard format showing authors, title, journal, issue, pages, and date, for each category list the following:

a) Papers published in peer-reviewed journals:

Dong-Hun Kim, Loon-Seng Tan, and Soo-Young Park, “Preparation of water-dispersible graphene using N-methylmorpholine N-oxide monohydrate and its application for the preparation of nanocomposites using PEDOT”, Journal of Materials Chemistry C, 7105, 2015

b) papers published in non-peer-reviewed journals or in conference proceedings (N/A)

c) conference presentations, (N/A)

d) Manuscripts submitted but not yet published

Woo-Geun Jo, Dong-Hun Kim, Loon-Seng Tan, and Soo-Young Park, “Polypyrrole nanocomposite with water-dispersible graphene”

e) Provide a list any interactions with industry or with Air Force Research Laboratory scientists or significant collaborations that resulted from this work.

1. We discussed our works with Dr. Loon-Seng Tan. He gave us valuable tips on the preparation of GPN and revise our manuscript for publication
2. We sent to our samples to Dr. Loon-Seng Tan for ink-jet printing applications.